โครงสร้างและความเป็นกรดของเอสแซดเอสเอ็ม-5 ที่มีอัตราส่วนซิลิกาต่ออะลูมินัมเท่ากับ 47 และ 95

นาย อุกฤษฎ์ พุ่มพับ

วิทยานิพนธ์นี้เป็นส่วนหนึ่งของการศึกษาตามหลักสูตรปริญญาวิทยาศาสตรมหาบัณฑิต
สาขาวิชา ปิโตรเคมีและวิทยาศาสตร์พอลิเมอร์
คณะวิทยาศาสตร์ จุฬาลงกรณ์มหาวิทยาลัย
ปีการศึกษา 2547
ISBN 974-17-6199-6

STRUCTURES AND ACIDITIES OF HZSM-5 WITH Si/Al RATIOS OF 47AND 95

Mr. Ukrid Poompub

A Thesis Submitted in Partial Fulfillment of the Requirements
for the Degree of Master of Science in Petrochemistry and Polymer Science
Faculty of Science
Chulalongkorn University
Academic Year 2004

ISBN 974-17-6199-6

Thesis title	STRUCTURES AND ACIDITIES OF HZSM-5 WITH Si/Al RATIOS OF 47AND 95
By	Mr. Ukrid Poompub
Field of Study	Petrochemical and Polymer Science
Thesis Advisor	Associate Professor Vudhichai Parasuk

Accepted by the faculty of science, Chulalongkorn University in Partial Fulfillment of the Requirements for the Master's Degree

..... Dean of the Faculty of Science
(Professor Piamsak Menasveta, Ph.D.)

THESIS COMMITTEE

..... Chairman
(Professor Pattarapan Prasassarakich, Ph.D.)

..... Thesis Advisor
(Associate Professor Vudhichai Parasuk, Ph.D.)

..... Member
(Associate Professor Supot Harnnongbua, Ph.D.)

..... Member
(Associate Professor Wimonrat Trakarnpruk, Ph.D.)

..... Member
(Aticha Chaisuwan, Ph.D.)

อุกฤษฎ์ พุ่มพับ: โครงสร้างและความเป็นกรดของเอสแซดเอสเอ็ม-5 ที่มีอัตราส่วนซิลิกอนต่ออะลูมินัมเท่ากับ 47และ 95 (STRUCTURES AND ACIDITIES OF HZSM-5 WITH Si/Al RATIOS OF 47 AND 95) อาจารย์ที่ปรึกษา: รศ.ดร. วุฒิชัย พาราสุข, 98หน้า, ISBN 974-17-6199-6

แซดเอสเอ็ม-5 (ZSM-5) เป็นตัวเร่งปฏิกิริยาที่มีการใช้กันอย่างกว้างขวางในอุตสาหกรรมปิโตรเคมี ความว่องไวในการเร่งปฏิกิริยาของ H-ZSM-5 ขึ้นอยู่กับความเป็นกรดของมัน งานวิจัยนี้ศึกษาความเป็นกรดของเอชแซดเอสเอ็ม-5 (H-ZSM-5) ที่มีอัตราส่วนซิลิกอนต่ออะลูมินัม (Si/Al) ต่างกัน 2 ค่าคือ 95 (แทนที่ Si 1ตำแหน่ง ด้วย Al 1 อะตอม) และ 47 (แทนที่ Si 2 ตำแหน่ง ด้วย Al 2อะตอม) การเตรียมและหาโครงสร้างเสถียรของเอชแซดเอสเอ็ม-5 ที่มีอัตราส่วนซิลิกอนต่ออะลูมินัมเท่ากับ 95 และ 47 และที่รูปแบบการแทนที่ต่างๆ ทำโดยใช้วิธีโมเลคิวลาร์ไดนามิกส์ (MD) ระยะของ $O...H^+$ ที่เป็นไปได้มากที่สุด มีระยะทาง 0.982 ถึง 0.998 อังสตรอม (Å) สำหรับเอชแซดเอสเอ็ม-5 ที่มีอัตราส่วนซิลิกอนต่ออะลูมินัมเท่ากับ 95 ขณะที่แซดเอสเอ็ม-5 ที่มีอัตราส่วนซิลิกอนต่ออะลูมินัมเท่ากับ 47 มีค่าเหล่านี้อยู่ในช่วง 0.986 ถึง 1.000 อังสตรอม ระยะ $O...H^+$ ที่ได้จากทุกตำแหน่งแทนที่มีระยะค่อนข้างสั้นและอยู่ในช่วงของพันธะ O-H ในน้ำ ดังนั้นโปรตอนสามารถเกิดพันธะเคมีกับออกซิเจนในซีโอไลต์ได้ การคำนวณโดยทฤษฎีทฤษฎีเดนซิตีฟังก์ชันนัล (DFT) B3LYP/6-31G (d, p) ได้ถูกนำมาใช้หาค่าโปรตอนแอฟฟินิตี (PA) ของเอชแซดเอสเอ็ม-5 และความเป็นกรดของมัน สำหรับเอชแซดเอสเอ็ม-5ที่มีอัตราส่วนซิลิกอนต่ออะลูมินัมเท่ากับ 95 ค่าโปรตอนแอฟฟินิตีอยู่ระหว่าง 388.8 ถึง 414.8 กิโลแคลอรีต่อโมล ตำแหน่งแทนที่ T5 ทีมีค่าโปรตอนแอฟฟินิตีต่ำที่สุดทำให้มันมีความเป็นกรดมากที่สุด ขณะที่เอชแซดเอสเอ็ม-5 ที่มีอัตราส่วนซิลิกอนต่ออะลูมินัมเท่ากับ 47 มีค่าโปรตอนแอฟฟินิตีอยู่ระหว่าง 391.8 ถึง 412.7 กิโลแคลอรีต่อโมล ตำแหน่ง T9 ในโครงสร้าง T9,T10 มีค่าโปรตอนแอฟฟินิตีต่ำที่สุดทำให้มันมีความเป็นกรดมากที่สุด เมื่อเปรียบเทียบความเป็นกรดของเอชแซดเอสเอ็ม-5 ที่มีอัตราส่วนซิลิกอนต่ออะลูมินัมเท่ากับ 95 และ 47 เห็นได้ว่าทุกตำแหน่งแทนที่ของการแทนที่อะลูมินัมที่มีอัตราส่วนซิลิกอนต่ออะลูมินัมเท่ากับ 95 มีความเป็นกรดสูงกว่าที่อัตราส่วน 47 ดังนั้นเอชแซดเอสเอ็ม-5ที่มีอัตราส่วนซิลิกอนต่ออะลูมินัมสูงกว่าจะเป็นกรดมากกว่าสอดคล้องกับผลการทดลอง อย่างไรก็ดีเราพบว่าที่ตำแหน่งแทนที่ T12 แซดเอสเอ็ม-5ที่มีอัตราส่วนซิลิกอนต่ออะลูมินัมเท่ากับ 47 มีความเป็นกรดมากกว่าแซดเอสเอ็ม-5ที่มีอัตราส่วนซิลิกอนต่ออะลูมินัมเท่ากับ 95

ภาควิชา.....-.....ลายมือชื่อ.....อุกฤษฎ์ พุ่มพับ.....

สาขาวิชา.....ปิโตรเคมีและวิทยาศาสตร์พอลิเมอร์.....ลายมือชื่ออาจารย์ที่ปรึกษา.....

ปีการศึกษา.....2547.....

4472507223: MAJOR PETROCHEMISTRY

KEYWORDS: H-ZSM-5 / Molecular Dynamic Simulation / Density Functional Theory / Proton Affinity / Acidity

UKRID POOMPUB: STRUCTURES AND ACIDITIES OF HZSM-5 WITH Si/Al RATIOS OF 47AND 95. THESIS ADVISER: ASSOC. PROF. VUDHICHAI PARASUK, Ph.D., 98pp. ISBN 974-17-6199-6

ZSM-5 catalyst is widely used in petrochemical industry. Its catalytic activity depends on its acidity. Investigation on the acidity of H-ZSM-5 with 2 different Si/Al ratios, *i.e.* 95 (monosubstituted) and 47 (disubstituted) were carried out. Using Molecular Dynamic Simulation (MD), structures of H-ZSM-5 at the Si/Al ratios of 95 and 47 and various substitution patterns were prepared and minimized. The most probable O…H^+ distances were found to be of 0.982 to 0.998 Å for ZSM-5 with the Si/Al ratio of 95, while H-ZSM-5 with the Si/Al ratio of 47 has these distances in the range of 0.986 to 1.000 Å. The O...H^+ distances obtained for all sites are rather short in the range of O-H bond in water. Thus H^+ forms chemical bond with the zeolitic O. Density functional theory (DFT) B3LYP/6-31G (d, p) calculations were used for determination of proton affinity (PA) of HZSM-5 and thus its acidity. For H-ZSM-5 with the Si/Al ratio of 95, the value of PA is between 388.8 and 414.8 kcal/mol. The T5 substitution has the lowest PA and hence most acidic. While H-ZSM-5 with the Si/Al ratio of 47, the value of PA are between 391.8 and 412.7 kcal/mol. The T9-site in T9, T10 model has lowest PA which makes it highest acidity. Compared acidity between H-ZSM-5 with the Si/Al ratios of 95 and 47, it could be observed that all Al substitutions at Si/Al ratio of 95 have higher acidity (lower PA) than those of 47 ratio. Thus, H-ZSM-5 with higher Si/Al ratio is more acidic in agreement with experiment. However, we have found that T12-site in ZSM-5 with the Si/Al ratio of 47 is more acidic than that with the Si/Al ratio of 95.

Field of study. Petrochemical and Polymer Science. Student's signature.....

Academic year.....2547..... Advisor's signature.....Vudhichai Parasuk.....

ACKNOWLEDGEMENTS

This thesis would not have been finished without contributions from many persons who helped me to overcome extensive hindrances and difficulties during my study. Truly, I cannot acknowledge the names of all, individually, who either directly or indirectly give me a help, or would like to apologize to them whom I fail to mention.

I would like to express my deepest appreciation and grateful thank to my thesis advisor, Associate Professor Dr. Vudhichai Parasuk for his concern, encouragement and valuable advice throughout my study.

I also would like to thank the Austrian-Thai Center for Computer Assisted Chemical Education and Research (ATC) and Computational Chemistry Chemical Unit Cell, Chulalongkorn University for computer resources and other facilities.

Finally, I would like to give all gratitude to my beloved parents for all their love, support and encouragement during the whole period of my study and for always letting me choose my own path.

CONTENTS

Pages

Pages

Pages

LIST OF FIGURE

Figure Pages

LIST OF TABLES

LIST OF ABBREVIATIONS

ZSM-5	Zeolite Scolony Mobil-5
MFI	Mobil Five
MD	Molecular Dynamic simulation
RDF	Radial Distribution Function
DFT	Density Functional Theory
PA	Proton Affinity
T-site	Tetrahedral-site
SBU	Secondary Building Unit
HF	Hatree-Fock Method
MO	Molecular Orbital
STO	Slater Type Orbital
GTO	Gaussian Type Orbital
DZ	Double Zeta
SCF	Self-Consistent Field
KS	Kohn-Sham
LDA	Local Density Approximation
LSDA	Local Spin Density Approximation
VWN	Vosko, Wilk and Nusair
GGA	Generalized Gradient Approximation
PW86	Perdew and Wang in 1986
PW91	Perdew and Wang in 1991
PW92	Perdew and Wang in 1992
B88	Becke in 1988
ACF	Adiabatic Connection Formula
ACM	Adiabatic Connection Model
B3LYP	Becke's 3 parameters and Lee-Yong-Parr for the correlation
ps	Pico-Second
ns	Nano-Second

CHAPTER 1

INTRODUCTION

Zeolites are microporous aluminosilicates that are industrially important for their catalytic and molecular sieving properties.[1,2] Some important catalytic applications include catalysts for petroleum refining, synfuel production, and petrochemical production. Their network of cavities and channels allows them to accommodate even moderately large molecules, and the presence of Al-substituted tetrahedral sites, with an associated H^+ being bound to a nearby O atom to maintain charge neutrality, results in acidic properties useful in catalysis. Classical Brønsted and Lewis acid model of acidity has been used to classify the active sites on zeolites.[3,4] Brønsted acidity is proton donor acidity; a trigonally coordinated alumina atom is an electron deficient and can accept an electron pair, therefore behaves as a Lewis acid. The nature of the distribution of aluminum over the framework cation sites in aluminosilicate zeolites is known to influence their catalytic performance.[5,6] In general, the increase in Si/Al ratio will increase acidic strength and thermal stability of high silica zeolite. Since the number of acidic OH groups depends on the number of aluminum in zeolite's framework, decrease in Al content is expected to reduce catalytic activity of zeolite.

H-ZSM-5, a synthetic zeolite currently accessible over a framework composition range $8 < Si/Al < \infty$, typically Si/Al = 25-100, is arguably the most technologically important zeolite.[7] Examples of its use include the conversion of methanol to gasoline, dewaxing of distillates, and the interconversion of aromatic compounds. Also, ZSM-5 has been shown to process unusual hydrophobicity, leading to potential applications in the separation of hydrocarbons from polar compounds, such as water and alcohol. The general framework structural characteristics of ZSM-5 (MFI-framework) and the closely related purely siliceous material silicalite are well-known. Silicate tetrahedra are interlinked to form 4-, 5- and 6-ring in characteristic pentasil cages and chains. The chain interconnections define a two-dimensional system of 10-ring channels, straight along [010], but sinusoidal along [100].

It is clear that experimental techniques are lacking in some respects in the determination of zeolite structure and that other methods are needed to complete the picture.[8] Computational modeling is an ideal candidate to bridge this gap. Computational methods have proven to be invaluable in this area especially when used in collaboration with experimental work to verify the results. The majority of work published today in the zeolite field has some sort of theoretical calculation associated with it in one form or another. In cases where spectroscopic and crystallographic methods have failed to completely resolve a crystal structure, empirical force field method have been used for calculation of minimum structures with aluminums explicitly placed.

Molecular or lattice dynamics techniques have been used for measurement of sorption process through the zeolite pore channels. Electronic structure methods have also been used on small clusters for elucidation of reaction pathways so that our understanding of zeolite chemistry can be increased with the aim of being able to predict how structural change will affect reactions.

The effects of local composition and structure on the acidity of ZSM-5 have recently been investigated by means of quantum mechanical calculations.[9] The calculation based on quantum density functional theory (DFT) are particularly well suited for assessing such effect on the electronic properties of Brønsted acid sites in H-ZSM-5 and other zeolites.[10] Such calculations have also been used for demonstration of that defects in the form of silanol groups located on a Si atom bonded via a bridging oxygen atom to an Al atom can significantly lower the proton affinity (PA) of the associated Brønsted acid proton. In many studies the strength of the Brønsted acid site is most often characterized by the PA, which is defined as the energy difference between the geometry optimized protonated and deprotonated (anionic) forms of the zeolite. It should be noted that PA provides one measurement of acidity, since the effects of differing conjugate base strength are completely ignored.

In this work, acidities of ZSM-5 with the Si/Al ratios of 47 and 95 were studied. Molecular dynamic simulations (MD) of ZSM-5 with the Si/Al ratios of 47 and 95 were performed. The cluster models of difference substitution tetrahedral-sites (T-site) were made from structures obtained from MD. The proton affinity (PA) of each model was computed to compare acidity between different (T-sites).

1.1 Zeolites

The history of zeolites began in 1976 when the Swedish mineralogist Constedt discovered the first zeolite mineral. The word “zeolite” derived from two Greek words “zeo” and “lithos” meaning “to boil” and “a stone”. Union Carbide Corporation discovered a number of commercially significant zeolites, type A, X and Y, during their research in 1948 to 1954. In 1967 to 1969, Mobil oil reported the synthesis of high silica zeolite beta and ZSM-5. Zeolites and molecular sieves are finding applications in many areas of catalysts. Zeolites exhibits appreciable acid activity with shape-selective feature not available in the compositional equivalent amorphous catalysts. In addition, these materials can act as supports for numerous catalytically active metals. They also have ion-exchange properties which allow performing all sorts of ion-exchanged reactions.[11]

For crystallite molecular sieves, McBain proposed the term “molecular sieve” to describe a class of materials that exhibited selective adsorption properties in 1932. He reported that for a material to be a molecular sieve, it must separate components of a mixture on the basis of molecular size and shape differences. Two classes of molecular sieves were known when McBain put forth his definition: the zeolites and certain microporous charcoals. The list now includes the silicates, the metallosilicates, metalloaluminates, the $AlPO_4$’s, and silico- and metalloaluminophosphates, as well as the zeolites. The different classes of molecular sieve materials are listed in Figure 1.1. All are molecular sieves, as their regular framework structures will separate components of a mixture on the basis of size and shape. The difference lies not within the structure of these materials, as many are structurally analogous, but in their elemental composition. Therefore, all are molecular sieve though none but the aluminosilicates should carry the classical name, zeolite.[12]

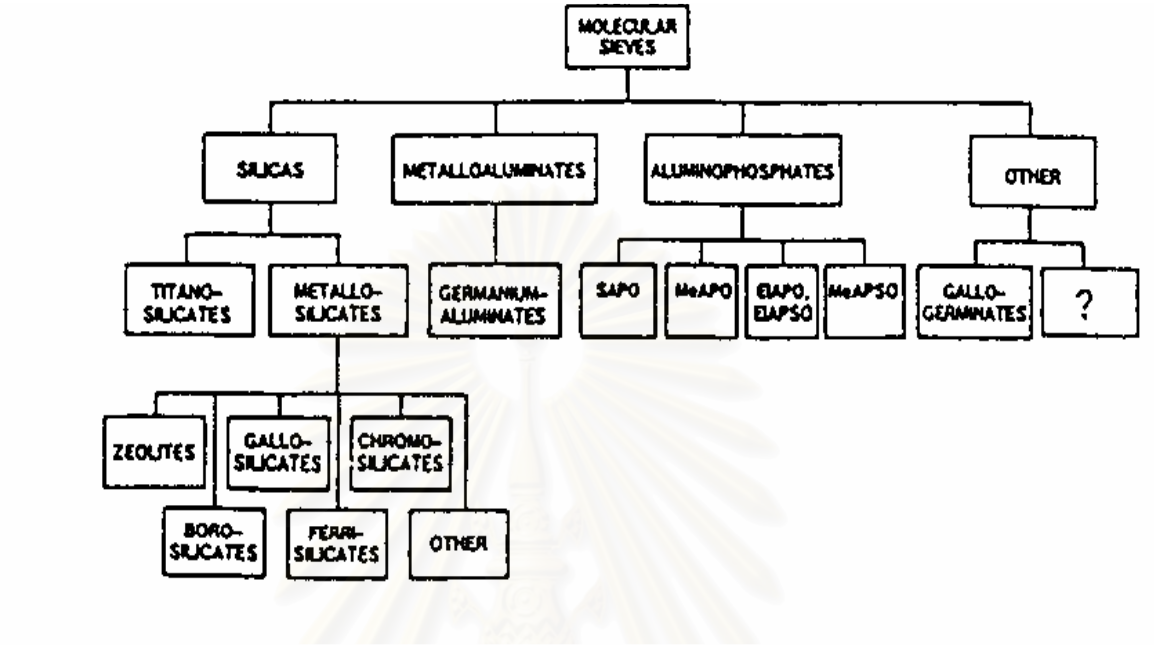

Figure 1.1 Classification of molecular sieve materials indicating extensive variation in composition

1.1.1 Structure of Zeolite

The structure of zeolite consist of a three-dimensional framework of $[SiO_4]^{4-}$ and $[AlO_4]^{5-}$ tetrahedra (Figure 1.2), each of which contains a silicon or aluminum atom in the center. The oxygen atoms are shared between adjoining tetrahedral, which can be present in various ratios and arranged in a variety of way. The framework obtained contains pores, channels and cages or interconnected voids. Zeolites may be represented by the general formula:

$$M_{x/n}[(AlO_4)_x(SiO_2)_y]wH_2O$$

Where the term in brackets is the crystallographic unit cell. The metal cation of valency n is present to produce electrical neutrality since for each aluminum tetrahedron in the

lattice there is an overall charge of -1. If M is a proton, the zeolite becomes a strong Brønsted acid. As catalyst, zeolite becomes a strong Brønsted acid. As catalyst, zeolites are unique in their ability to discriminate between reactant molecular size and shape.

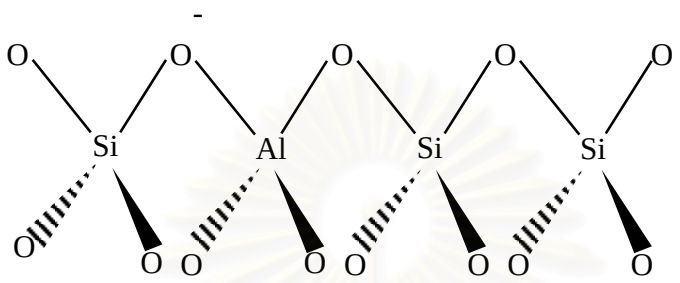

Figure 1.2 The linkage of primary building unit of $[SiO_4]^{4-}$ and $[AlO_4]^{5-}$ tetrahedra.

All zeolites are significant for catalytic and adsorbent applications can be classified by the number of T atoms, where T = Si or Al, that define the pore opening. There are three pore openings known to date in the aluminosilicate zeolite system that are practically of interest for catalytic applications; they are descriptively referred to as 8-, 10-, and 12-ring openings. Zeolites containing these pore openings may also be referred to as small (8-member ring), medium (10-member ring) and large (12-member ring) pore zeolites. In this simplified classification system, no indication is given as to exact dimension of the pore opening or whether the zeolite contains a one-, two-, or three-dimensional pore system. The different ring sizes, based on the different number of T atoms defining the opening, are shown in Figure 1.3 for three representative zeolites: erionite, ZSM-5 and type-Y zeolites of known structure are listed in Table 1.1, classified in terms of their largest pore opening. Generally one can consider any of the zeolites in the individual classes to provide similar shape-selective behavior.

Table 1.1 Known zeolite structures listed by pore opening, as defined as the number of T (or TO_4) units that shape the channels.

8-ring	10-ring	12-ring
Type A, ZK-5	ZSM-5 (Silicalite)	Faujasite (Type X and Y)
Bakitaite	ZSM-5	Mordernite
Brewsterite	Dachiardite	Cancrinite
Chabazite	Epistilbite	Gmerlinite
TMA-E (AB)	Ferrierite	Type L
Edingtonite	Laumanite	Mazzite
Erionite	Stilbite	Offertite
Gismondine	ZSM-23	Omega
Heulandite	Theta-1 (ZSM-22)	ZSM-12
Levyne	Eu-1 (ZSM-50)	Beta
Merlinoite	Eu-2 (ZSM-48)	
Natrolite		
Phillipsite		
Paulingite		
Rho		
Thomsonite		
Yugawaralite		

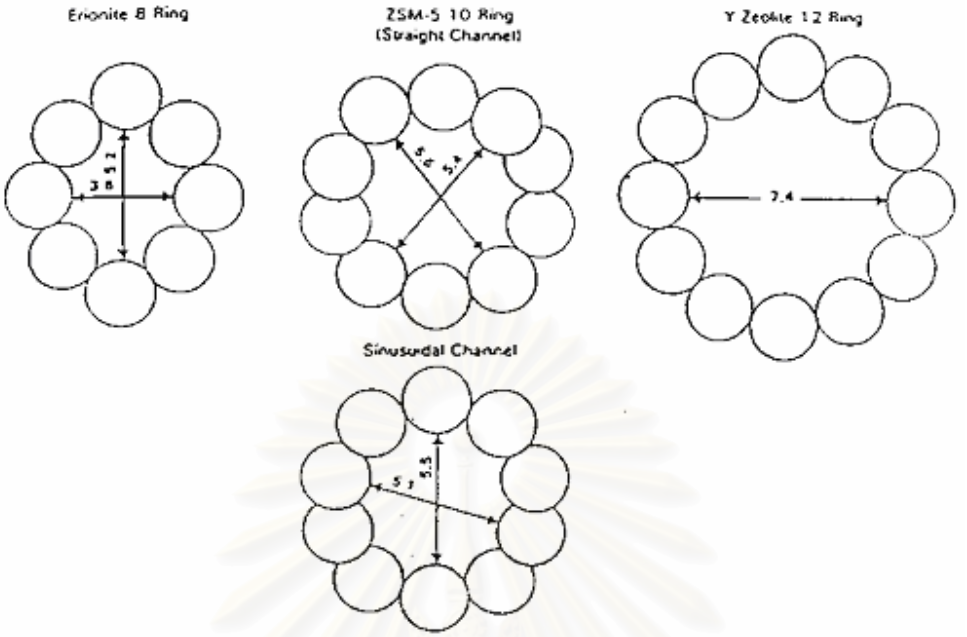

(a)

(b)

Figure 1.3 Examples of the three types of pore opening in the zeolite molecular sieves. (a) Erionite contains an 8 ring pore opening; ZSM-5, two 10 ring systems differing in shape of the opening; and type Y zeolite, a 12-ring pore system. (b) Front and side views of the pore opening for erionite.

The primary building unit of a zeolite structure is the individual tetrahedral TO_4 unit, where T is either Si or Al. A secondary building unit (SBU) consists of selected geometric groupings of those tetrahedral. There are nine such building units, which can be used to describe all of known zeolite structures. These secondary building units consist of 4 or (S4R), 6 or (S6R), and 8 or (S8R)-member single ring, 4-4 or (D4R), 6-6 or (D6R), 8-8 or (D8R)-member double rings, and 4-1, 5-1 and 4-4-1 branched rings. The topologies of these units are shown in Figure 1.4. Also listed are the symbols used to describe them. Most zeolite framework can be generated from several different SBU's.

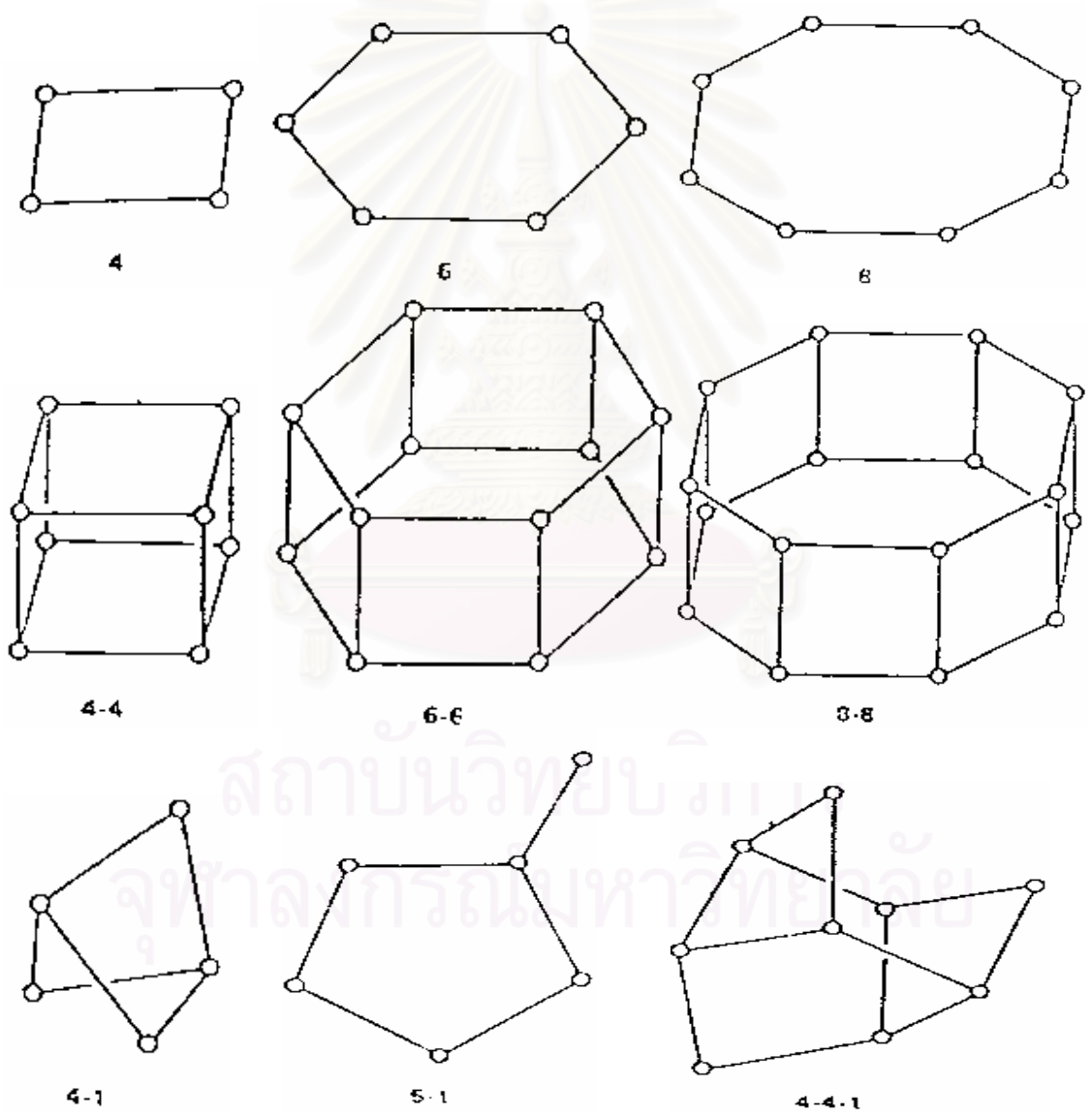

Figure 1.4 Secondary building unit (SBU's) found in zeolite structures.

The framework of zeolites used most frequently as adsorbent or catalyst is shown in Figures 1.5(a)-1.5(c) The Al or Si atoms are located at the intersection of lines that represent oxygen bridges. The X and Y zeolites are structurally and topologically related to the mineral faujasite and frequently refered to as faujasite-type zeolites. The two materials differ chemically by their Si/Al ratios, which are 1-1.5 and 1.5-3.0 for X and Y zeolite, respectively. In faujasites, large cavities of 1.3 nm in diameter (supercages) are connected to each other through apertures of 1.0 nm.[14]

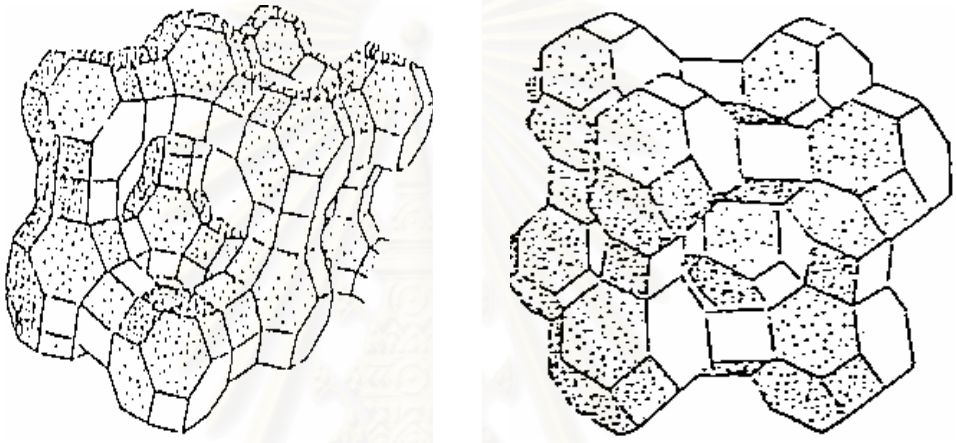

(a) (b)

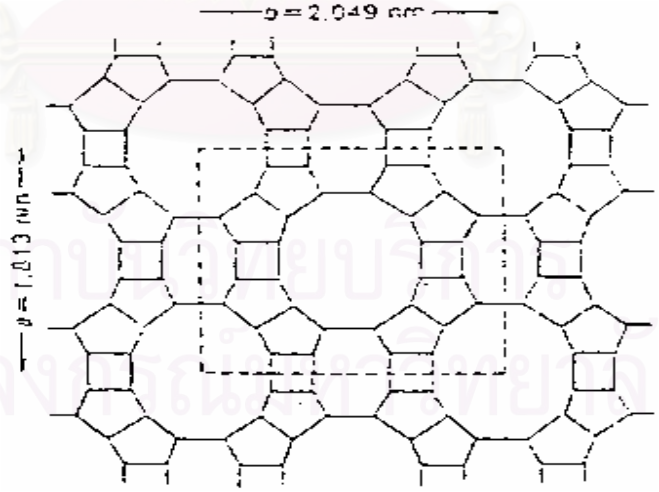

(c)

Figure 1.5 Structure and skeleton diagram of varies zeolites; (a) Structure of type-Y (or X) zeolite; (b) Structure of type-A zeolite; (c) Skeleton diagram of the (001) face of modernite.

1.1.2 Ion-exchange Reaction in Zeolites

The cation exchange property of zeolite mineral was first observed in 19th century. The ease of cation exchange in zeolites and other minerals led to an early interest in ion exchange materials for use as water softening agents. Nowadays, it is found that ion-exchange is the simplest and most important for modifying the properties of zeolite. Zeolites are normally prepared in the Na form, and this can be changed to NH_4 form and also followed by heat treatment to produce H-form zeolite. The equations of these treatments are

$$\text{Na-Zeolite} + NH_4^+ \longrightarrow NH_4\text{-Zeolite} + Na^+ \qquad (1.1)$$

$$NH_4\text{-Zeolite} \xrightarrow{\text{heat}} \text{H-Zeolite} + NH_3 \qquad (1.2)$$

The transition metal exchanged zeolites could be prepared as well. The procedure which is certainly the most suitable in introducing cation into the zeolite framework, consist of exchanging the primary cation, such as Na^+ or NH_4^+ and so on, with a solution of the metal salt, through conversion ion-exchange technique as shown in Figure 1.6 and the equation below:[15]

$$(Na)^+_n\text{-Zeol} + Me^{n+}(H_2O)\,X \longrightarrow Me^{n+}(H_2O)\text{-Zeol} + nNa^+ \qquad (1.3)$$

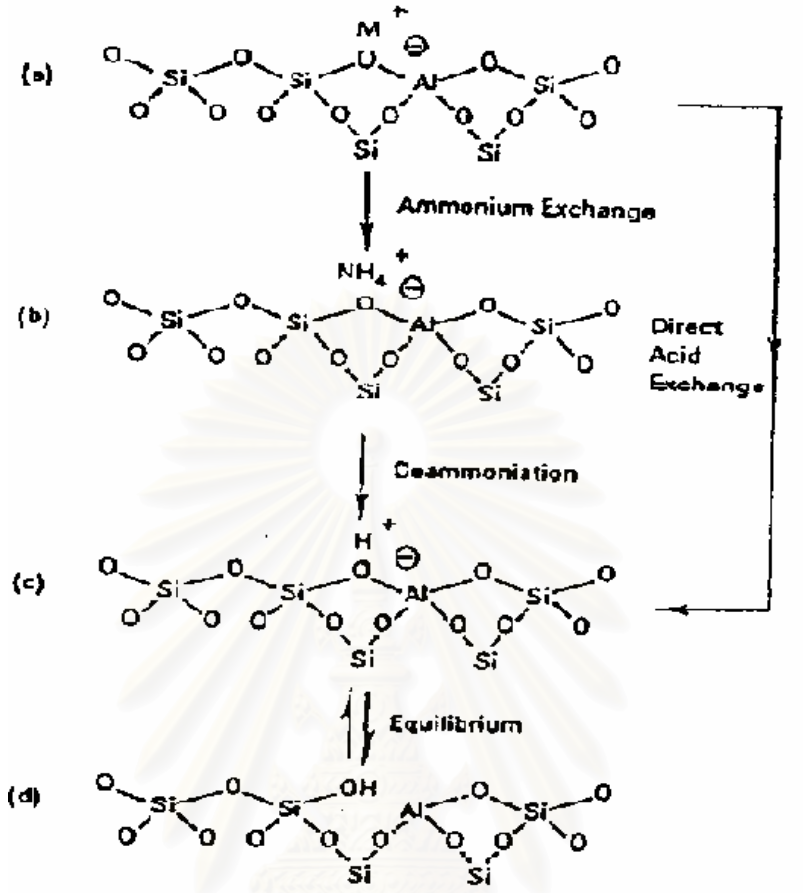

Figure 1.6 Diagram of the structure of a zeolite framework.[16]

(a) In the as-synthesized form M^+ is either an organic cation or an alkali metal cation.

(b) Ammonium ion exchange produces the NH_4^+ exchanged form.

(c) Thermal treatment is used for removal of ammonia, producing the H^+ acid form.

(d) The acid form in (c) is in equilibrium with the form shown in (d), where there is a silanol group adjacent to a tricoordinate aluminum.

The cation exchange behavior of zeolites depends upon

1) The number of the cation species, the cation size, both anhydrous and hydrated, and cation exchange.

2) The temperature.
3) The concentration of the cation species in solution.
4) The anion species associated with the cation in solution.
5) The solvent (most exchange has been carried out in aqueous solutions, although some work has been done in organic solvents).
6) The structural characteristics of the particular zeolite.

Cation selectivities in zeolites do not follow the typical rules that are evidenced by other inorganic and organic exchangers. Zeolite structures have unique features that lead to unusual types of cation selectivity and sieving. The recent structural analyses of zeolites are from a basis for interpreting the variable cation exchanger behavior of zeolites.

Cation exchange in zeolite is accompanied by dramatic alteration of stability, adsorption behavior and selectivity, catalytic activity and other important physical properties. Since many of these species, detailed information on the cation exchange equilibria is important. Extensive studies of the ion exchange process in some of the more important mineral and synthetic zeolites have been conducted.

1.1.3 Shape Selectivity

Many reactions involving carbonium ions intermediates are catalyzed by acidic zeolites.[23] With respect to a chemical standpoint the reaction mechanisms are not fundamentally different with zeolites or with any other acidic oxides. The shape selective characteristics of zeolites influence their catalytic phenomena by three modes; reactant, product and transition state shape selectivity. These types of selectivity are depicted in Figure 1.7.

Reactant or charge selectivity occurs as slowly diffusing product molecules can not escape from the crystal and undergo secondary reactions. This reaction path is established by monitoring changes in product distribution as a function of varying contact time.

Restricted transition state shape selectivity is a kinetic effect arising from local environment around the active site, the rate constant for a certain reaction mechanism is reduced if the necessary transition state is too busy to form readily.

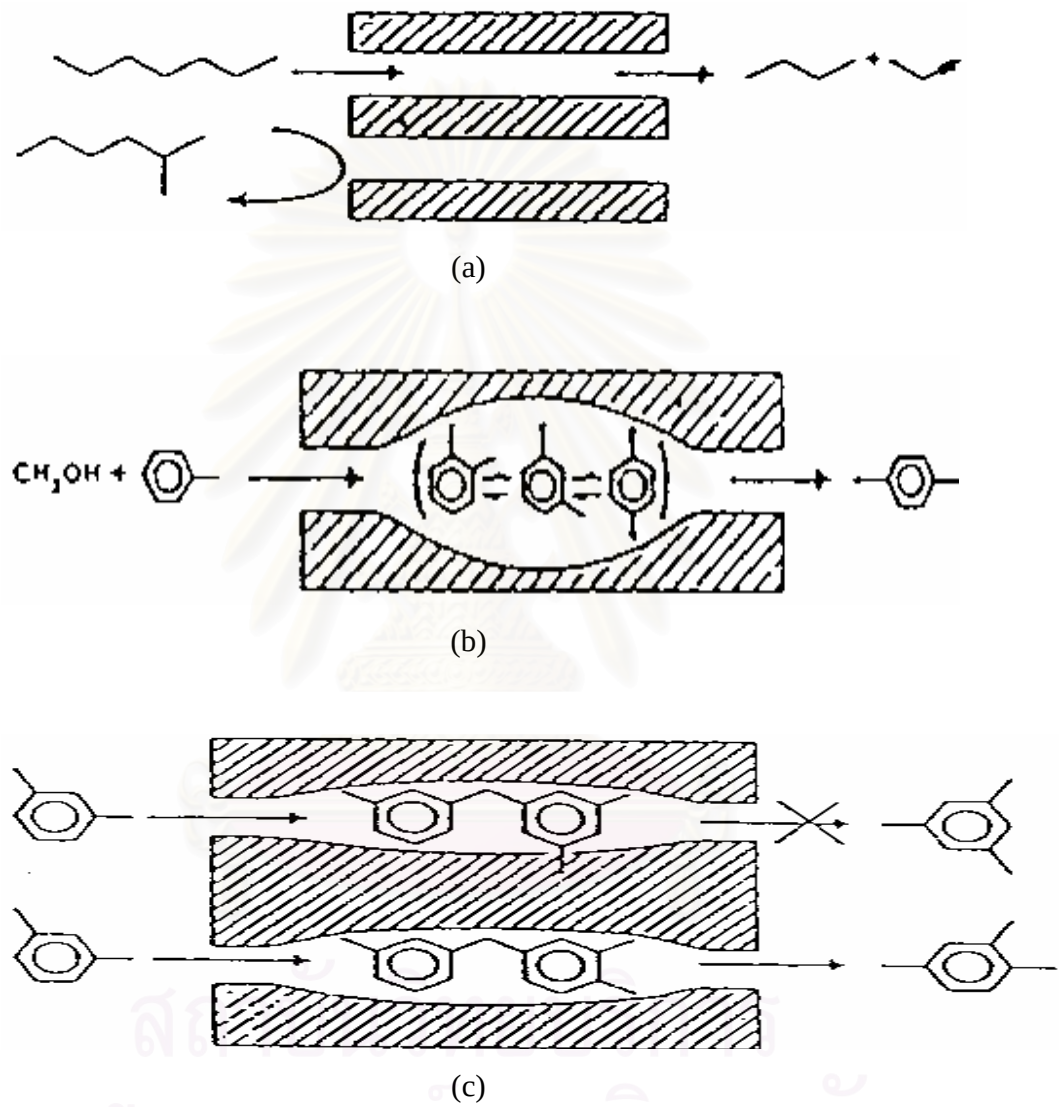

Figure 1.7 Diagram of (a) reactant shape selectivity in channels of zeolite A; (b) Product shape selectivity in ZSM-5 channels; (c) Transition state shape selectivity in mordenite channels.[17]

The critical diameter (as apposed to the length) of the molecules and the pore channel diameter of zeolite are important in predicting shape selective effects. However, molecules are deformable and can pass through openings which are smaller than their critical diameters. Hence, not only size but also the dynamics and structure of the molecules must be taken into account. Table 1.2 present values of selected critical molecular diameters and Table 1.3 present values of the effective pore size of structure of various zeolites. Correlation between pore size(s) of zeolites and kinetics diameter of some molecules are depicted in Figure 1.8.

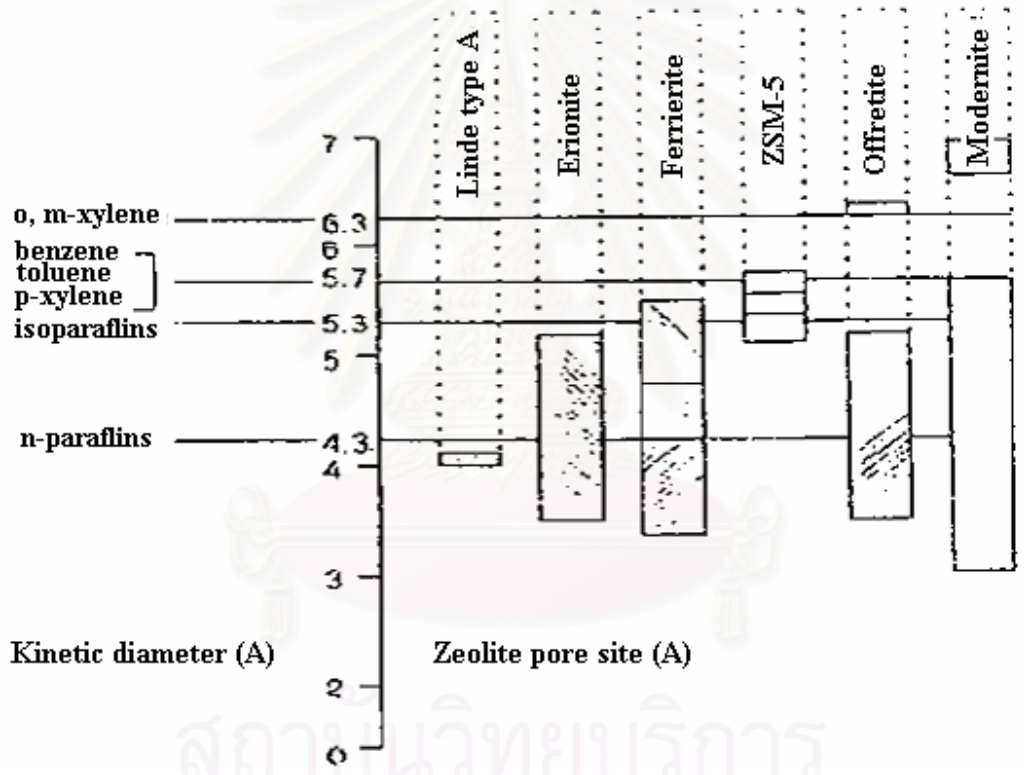

Figure 1.8 Correlation between pore size(s) of various zeolites and kinetic diameters of some molecules.

Table 1.2 Kinetic diameter of various molecules based on the Lennard-Jones relationship.

	Kinetic Diameter (Angstroms, Å)
He	2.60
H_2	2.89
O_2	3.46
N_2	3.64
NO	3.17
CO	3.76
CO_2	3.30
H_2O	2.65
NH_3	2.60
CH_4	3.80
C_2H_2	3.30
C_3H_8	4.30
n-C_4H_{10}	4.30
Cyclopropane	4.23
i-C_4H_{10}	5.00
n-C_5H_{12}	4.90
SF_6	5.50
Neopentane	6.20
$(C_4F_9)_3N$	10.20
Benzene	5.85
Cuclohexane	6.00
m-xylene	7.10
o-xylene	7.40
p-xylene	6.75
1,3,5-trimethylbenzene	8.50
1,3,5-triethylbenzene	9.20
1-methylnaphthalene	7.90
$(C_4H_9)_3N$	8.10

Table 1.3 Shape of the pore mount openings of known zeolite structures, The dimensions are based on two parameters, the number of T atoms forming the channel opening (8-, 10-, 12-rings) and the crystallographic free diameters of the channels. The channels are parallel to the crystallographic axis shown in brackets (e.g. [100].[18]

STRUCTURE	8 MEMBER RING	10 MEMBER RING	12 MEMBER RING
Bakitaite	3.2 × 4.9[001]		
	2.3 × 5.0[100]		
	2.7 × 4.1[001]		
Cancrinite			6.2[001]
Chabazite	3.6 × 3.7[001]		
Dachiardite	3.6 × 4.8[001]	3.7 × 6.7[010]	
TMA-E	3.7 × 4.8[001]		
Edingtonite	3.5 × 3.9[110]		
Epistillbite	3.7 × 4.4[001]		
Erionite	3.6 × 5.2[001]		
Faujasite			7.4[111]
Ferrierite	3.4 × 4.8[010]	4.3 × 5.5[001]	
Gismondine	3.1 × 4.4[010]		
	2.8 × 4.9[010]		
Gmelinite	3.6 × 3.9[001]		7.0[001]
Heulandite	4.0 × 5.5[100]	4.4 × 5.5[001]	
	4.1 × 4.7[001]		
ZK-5	3.9[100]		
Laumonite		4.0 × 5.6[100]	
Levyne	3.3 × 5.3[001]		
Type A	4.1[100]		
Type L			7.1[001]
Mazzite			7.4[001]
ZSM-11		5.1 × 5.5[100]	
ZSM-5		5.4 × 5.6[010]	
		5.1 × 5.5[100]	
Modernite	2.9 × 5.7[010]		6.7 × 7.0[001]
Natrolite	2.6 × 3.9[101]		
Offretite	6.5 × 5.2[001]		6.4[001]
Paulingite	3.9[100]		

1.1.4 Zeolite Active Size

1.1.4.1 Acidity of Zeolite

Based on electrostatic consideration, the charge density at a cation site increases with increasing Si/Al ratio. It was conceived that these phenomena are related to the reduction of electrostatic interaction between framework sites, and possibly to the difference in the order of aluminum in zeolite crystal and the location of Al in crystal structure.[19]

Recently it has been reported that the mean charge on the proton was shifted regularity forward higher values as the Al content decreased.[20]Simultaneously the total number of acidic hydroxyls, governed by the Al atoms, was decrease. This evidence emphasized that the entire acid strength distribution (weak, medium, strong) was shifted towards stronger values. That is, weaker acid sites become stronger with the decrease in Al content.

An improvement in thermal or hydrothermal stability has been ascribed to the lower density of hydroxyl groups which parallel to that of Al content.[21]A longer distance between hydroxyl groups decreases the probability of dehydroxylation that generates defects on structure of zeolites.

1.1.4.2 Generation of Acid Centers

Most industrial application of zeolites are based upon technology adapted from the acid silica/alumina catalysts originally developed for the cracking reaction. This means that the activity required is based upon the production of Brønsted sites arising from the creation of “hydroxyl” within the zeolite pore structure. These hydroxyls are usually formed either by ammonium or polyvalent cation exchange followed by a calcinations step, that was already mentioned previously.[22]

In the case of zeolite catalyst, the source of acidity may be rationalized in term of a theory developed largely by Linus Pauling, if an aluminum ion, which is trivalent, is substituted isomorphously for silicon ion, which is quadrivalent, in a silica lattice comprising silica tetrahedral, the net negative charge must be stabilized by a nearby positive ion.

The exchange of monovalent ions by polyvalent cations could improve the catalytic property. Those highly charged cations create very acidic centres by hydrolysis phenomena.

Brønsted acid sites are also generated by the reduction of transition metal cations. The concentration of OH groups of zeolite containing transition metals was noted to increase by reduction with hydrogen at 250-450 °C and increase with the rise of the reduction temperature.

$$Cu^{2+} + H_2 \longrightarrow Cu^0 + 2H^+ \quad (1.4)$$

$$Ag+ + 1/2H_2 \longrightarrow Ag^0 + H^+ \quad (1.5)$$

1.1.5 ZSM-5

ZSM stands for “Zeolite Scolony-Mobil-5. ZSM-5 is currently one of the most interesting in industrially field. Its structures as shown in Figure 1.9, in which pores are shown as arrays of tubular channels. Two pore types exist, intersecting with each other, and both formed by 10-membered oxygen rings. One pore type has straight but slightly elliptical opening, the other zig-zag and essentially circular openings. The intersection provides an opening that in effect can provide a type of cavity. In additional, a material that is nearly pure silica, termed silicalite-1, has essentially the same structure as ZSM-5, while silicalite-s has the same structure as ZSM-11. [23]

The three-dimensional structure of silicalite-1 (MFI type catalyst) is represented in Figure 1.9 (a). The ten-membered rings provide access to a network of intersecting pores within the crystal. The pore structure of silicalite-1 (and ZSM-5) is presented in Figure 1.9 (b): there is a set of straight, parallel pores intersected by set of perpendicular

zigzag pores. Many molecules are small enough to penetrate into this intracrystalline pore structure, where they may be catalytically converted.

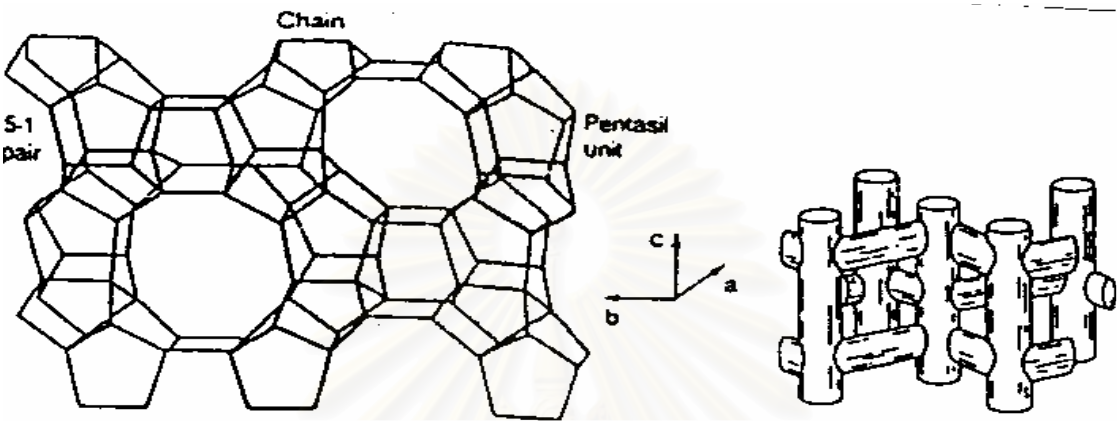

(a) (b)

Figure 1.9 Three dimensional structures of ZSM-5;
(a) Skeletal diagram of the (010) face of ZSM-5
(b) Channel network

In ZSM-5, the tetrahedra are linked to form the chain-type building block. The chains can form a layer as shown in Figure 1.10. Rings consisting of five O atoms are evident in this structure; the name pentasil is therefore used to describe it. Also evident in Figure 1.10 are rings consisting of 10 oxygen atoms; these are important because they provide openings in the structure large enough for passage of rather large molecules. The layers can be linked in two ways; the neighboring layers being related either by the operation of a mirror or an inversion. The former pertains to the silicalite-2 or ZSM-11, the latter to silicalite-1 or ZSM-5; the intermediates structure constitutes the pentasil series.

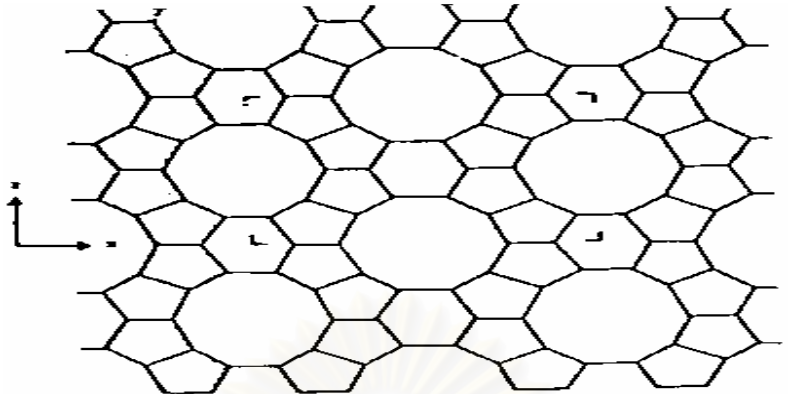

Figure 1.10 Schematic diagrams of silicalite layer, formed by linking of the chains through sharing of oxygen in linked SiO_4 tetrahedral.

1.2 The Objective of This Study

1 To investigate acidity of HZSM-5 with 2 different Si/Al ratios, *i.e.* 47 and 95.

2 To study the structural properties of H-ZSM-5 with the Si/Al ratios of 47 and 95, at the different T-sites.

3 To compare the acidity of all H-ZSM-5 structures with the Si/Al ratios of 47 and 95.

CHAPTER 2

THEORY

2.1 Schrödinger Equation

The Schrödinger equation is a fundamental equation of quantum mechanics. The solutions to the Schrödinger equation are called wave functions (Ψ). The main goal of quantum chemical calculation is to compute energy and other properties of molecule. These properties can be obtained by solving the Schrödinger equation [24]

$$\hat{H} \quad \Psi \quad = \quad E \quad \Psi \tag{2.1}$$

Here $\hat{H}$ is the Hamiltonian operator, a different operator representing the total energy. E is the numerical value of the energy of the state, that is, the energy relative to a state in which the constituent particles (nuclei and electrons) are infinitely separated and at rest. Ψ is the wave function. It depends on the coordinates of all particles and also on the spin coordinates. The square of wave function, Ψ^2 (or $|\Psi|^2$ if the Ψ is complex), is interpreted as a measure of the probability distribution of the particles within the molecule.

For a general N-particle the Hamiltonian operator contains kinetic ($\hat{T}$) and potential ($\hat{V}$) energy for all particles.

$$\hat{H} \quad = \quad \hat{T} \quad + \quad \hat{V} \tag{2.2}$$

For a molecule,

$$\hat{T} \quad = \hat{T}_n + \hat{T}_e \quad = - \sum_{A=1}^{N} \frac{1}{2M_A} \nabla_A^2 \; - \sum \frac{1}{2} \nabla_i^2 \tag{2.3}$$

where ∇_i^2 and ∇_A^2 is the Laplacian operators acting on electrons and nuclei, respectively.

And,

$$\hat{V} = \hat{V}_{ne} + \hat{V}_{ee} + \hat{V}_{nn} = -\sum_{i=1}^{n}\sum_{A=1}^{N}\frac{Z}{r_{iA}} + \sum_{i=1}^{n}\sum_{j\langle 1}^{n}\frac{1}{r_{ij}} + \sum_{A=1}^{N}\sum_{B\langle A}^{N}\frac{Z_A Z_B}{R_{AB}} \qquad (2.4)$$

From (2.2) to (2.4), the molecular Hamiltonian is,

$$\hat{H} = -\sum_{i=1}^{n}\frac{1}{2}\nabla_i^2 - \sum_{A=1}^{N}\frac{1}{2M_A}\nabla_A^2 - \sum_{i=1}^{n}\sum_{A=1}^{N}\frac{Z_A}{r_{iA}} + \sum_{i=1}^{n}\sum_{j>i}^{n}\frac{1}{r_{ij}} + \sum_{A=1}^{N}\sum_{B>A}^{N}\frac{Z_A Z_B}{R_{AB}} \qquad (2.5)$$

where A and B refer to nuclei, i and j refer to electrons. The first and second terms in (2.5) are the operator for the kinetic energy of the nuclei and electron, respectively. The third term is the electron-nuclear attraction where r_{iA} being the distance between electron i and nucleus A. The fourth term is the electron-electron repulsion where r_{ij} being the distance between electron i and j. The last term is the nuclei repulsion with atomic numbers Z_A and Z_B while R_{AB} being the distance between nuclei A and B, respectively.

2.2 The Born-Oppenhiemer Approximation

The Schrödinger equation cannot be solving exactly for any molecular systems. The first major step in simplifying the general molecular quantum mechanics is the separation of the nuclear and electronic motions. This is possible because the nuclear masses are much greater than those of the electrons therefore, nuclei move much more slowly. As a consequence, the electrons in a molecule adjust their distribution to changing nuclear position rapidly. This makes it reasonable approximation to suppose that the electron distribution depends only on the instantaneous positions of the nuclei and not on their velocities. [25]

In other words quantum mechanical problem of the electron motion in the field of fixed nuclei may first be solved leading to an effective electronic energy $E^{eff}(R)$ which depends on the relative nuclear coordinates, denoted by *R*. This effective energy is then used as a potential energy for a subsequent study of the nuclear motion. $E^{eff}(R)$ will depend on all of the relative nuclear coordinates. This separation of the general problem into two parts is frequently called the adiabatic or Born-Oppenheimer approximation. It was examine quantitatively by Born and Oppenheimer, who showed that it was valid, provided that the ratio of electron to nuclear mass sufficiently large.

Quantitatively, the Born-Oppenheimer approximation may be formulated by writing down the Schrödinger equation for electrons in the field of fixed nuclei,

$$\hat{H}^{elec}\Psi^{elec}(r,R) = E^{eff}(R)\Psi^{elec}(r,R) \tag{2.6}$$

where

$$\hat{H}^{elec} = -\sum_{i=1}^{N}\frac{1}{2}\nabla_i^2 - \sum_{i=1}^{N}\sum_{A=1}^{N}\frac{Z_A}{r_{iA}} + \sum_{i=1}^{N}\sum_{j>i}^{N}\frac{1}{r_{ij}} \tag{2.7}$$

The first part of (2.7) corresponds to the kinetic energy of the electrons only. The second term is the attraction of electron to nuclei. The third term is the repulsion between electrons. Here, Ψ^{elec} is the electronic wave function which depends on the electronic coordinates, *r*, as well as on the nuclear coordinates, R. E^{eff} is the eigenvalue of equation (2.6) called electric energy and depends parametrically on the nuclear coordinates, *R*.

The corresponding approximation to the total wave function is the multiplication product of electronic wave function $\Psi^{elec}(\{r_i\};\{R_A\})$, which describes the motion of the electrons that explicitly depends on the electronic coordinates, but parametrically depends on the nuclear coordinates and of nuclei wave function $\Psi^{nucl}(\{R_A\})$, which describes the vibration, rotation, and translation of a molecule.

$$\Psi(\{r_i\};\{R_A\}) = \Psi^{elec}(\{r_i\};\{R_A\})\Psi^{nucl}(\{R_A\}) \tag{2.8}$$

The total energy for fixed nuclei must also include the constant nuclear repulsion energy,

$$\varepsilon = E^{eff} + \sum_{A=1}^{M} \sum_{B>A}^{M} \frac{Z_A Z_B}{R_{AB}} \tag{2.9}$$

The total energy $\varepsilon(\{R_A\})$ provides a potential for nuclear motion. This function constitutes a potential energy surface.

The Born-Oppenheimer approximation is usually very good. For the hydrogen molecule the error is of the order of 10^{-4} a.u., and for systems with heavier nuclei, the approximation becomes better.

2.3 Hatree-Fock Approximation

The Hatree-Fock approximation (HF) breaks the many-electron Schrödinger equation into many simpler one-electron equations. Each one-electron equation is solved to yield a single-electron wave function, called an orbital, and an energy, called an orbital energy.

The simplest antisymmetric wave function, which can be used to describe the ground state of the an N-electron system, Ψ_0, is a single Slater determinant,

$$\Psi_0 = |\chi_1 \chi_2 \cdots \chi_a \chi_b \cdots \chi_N\rangle \tag{2.10}$$

where χ_i is the one-electron wave function and is the function and is the function of electron coordinates and spins. The wave function of (2.10) is also called Hatree-Fock wave function.

The electronic energy for HF approximation can be determined using.

$$E_0 = \langle \Psi_0 | \hat{H} | \Psi_0 \rangle \tag{2.11}$$

where $\hat{H}$ is the full electronic Hamiltonian. ε_0 is not the exact energy since Ψ_0 is not the exact wave function. To obtain the new ε_0, the variation principle is introduced. The variational flexibility in the wave function (2.10) is in the choice of spin orbitals, one can derive eigenvalue equation, called the *Hatree-Fock equation* which determines the optimal spin orbitals of the form,

$$f(i)\chi(x_i) = \varepsilon\chi(x_i) \tag{2.12}$$

where f(i) is an effective one-electron operator, called the *Fock operator*, of the form

$$f(i) = -\frac{1}{2}\nabla_i^2 - \sum_{A=1}^{M}\frac{Z_A}{r_{iA}} + V^{HF}(i) \tag{2.13}$$

where $V^{HF}(i)$ is the average potential experienced by the i^{th} electron due to the presence of the other electrons. The essence of the Hatree-Fock approximation is to replace the complicate many-electron problem by one-electron problem in which electron-electron repulsion is treated in an average way.

The Hartree-Fock potential $V^{HF}(i)$, or equivalently the "field" seen by the i^{th} electron, depends on the spin orbitals of the other electrons. Thus the Hartree-Fock equation (2.12) is nonlinear and must be solved iteratively. The procedure for solving the Hartree-Fock equation is called the *self-consistent-field* (SCF) method.

From equation (2.12), the best (Hatree-Fock) spin orbitals is the Hartree-Fock integro-differential equation

$$h(1)\chi_a(1) + \sum_{b\neq a}^{N}\left[\int dx_2 \left|x_b(2)\right|^2 r_{12}^{-1}\right]\chi_a(1) - \sum_{b\neq a}^{N}\left[\int dx_2 \chi_b^*(2) r_{12}^{-1}\rho_{12}\chi_b(2)\right]\chi_a(1) = \varepsilon_a\chi_a(1) \tag{2.14}$$

or

$$\left[h(1) + \sum_{b\neq a}^{N} J_b(1) - \sum_{b\neq a}^{N} K_b(1)\right]\chi_a(1) = \varepsilon_a\chi_a(1) \tag{2.15}$$

where h(1) is core-Hamiltonian operator

$$h(1) = -\frac{1}{2}\nabla_1^2 - \sum_{A=1}^{M}\frac{Z_A}{r_{1A}} \tag{2.16}$$

$J_b(1)$ is the coulomb operator

$$J_b(1) = \int dx_2 \left|\chi_b(2)\right|^2 r_{12}^{-1} \tag{2.17}$$

$K_b(1)$ is the exchange operator

$$K_b(1) = \int dx_2 \chi_b^*(2) r_{12}^{-1} P_{12}\chi_b(2) \tag{2.18}$$

Therefore, the Fock operator f(1) can be written as

$$f(1) = h(1) + \sum_{b=1}^{N}\left[J_a(1) - K_b(1)\right] \tag{2.19}$$

and the Hartree-Fock potential $V^{HF}(1)$,

$$V^{HF}(1) = \sum_{b=1}^{N}\left[J_a(1) - K_b(1)\right] \tag{2.20}$$

the orbital energy ε_a,

$$\varepsilon_a = \int \chi_a^* h \chi_a dx_1 + \sum_{b=1}^{N}\left[\int \chi_a^* \chi_a r_{12}^{-1} \chi_b^* \chi_b dx_1 dx_2 - \int \chi_a^* \chi_b r_{12}^{-1} \chi_b^* \chi_a dx_1 dx_2\right] \tag{2.21}$$

and Hartree-Fock energy

$$E_0 = \sum_{a=1}^{N}\int \chi_a^* h \chi_a dx_1 + \frac{1}{2}\sum_{a=1}^{N}\sum_{b=1}^{N}\left[\int \chi_a^* \chi_a r_{12}^{-1} \chi_b^* \chi_b dx_1 dx_2 - \int \chi_a^* \chi_b r_{12}^{-1} \chi_b^* \chi_a dx_1 dx_2\right] \tag{2.22}$$

$$E_0 = \sum_{a=1}^{N}\varepsilon_a \frac{1}{2}\sum_{a=1}^{N}\sum_{b=1}^{N}\left[\int \chi_a^* \chi_a r_{12}^{-1} \chi_b^* \chi_b dx_1 dx_2 - \int \chi_a^* \chi_b r_{12}^{-1} \chi_b^* \chi_a dx_1 dx_2\right] \tag{2.23}$$

For closed-shell restricted Hartree-Fock wavefunction (RHF)

$$\left|\Psi_0\right\rangle = \left|\chi_1\chi_2\chi_3\chi_4 \cdots \chi_{N-1}\chi_N\right\rangle$$

$$= \left|\Psi_1\overline{\Psi}_1\Psi_2\overline{\Psi}_2 \ldots \Psi_{N/2}\overline{\Psi}_{N/2}\right\rangle$$

$$E_0 = 2\sum_{a=1}^{N/2}\int \psi_a^* h \psi_a dx_1 + \sum_{a=1}^{N/2}\sum_{b=1}^{N/2}\left[2\int \psi_a^*\psi_a r_{12}^{-1}\psi_b^*\psi_b dx_1 dx_2 - \int \psi_a^*\psi_b r_{12}^{-1}\psi_b^*\psi_a dx_1 dx_2\right]$$

or
$$\mathrm{E}_0 = 2\sum_{a=1}^{N/2} h_{aa} + \sum_{a=1}^{N/2}\sum_{b=1}^{N/2}\left(2J_{ab} - K_{ab}\right) \qquad (2.24)$$

where $J_{ab} = \int \psi_a^*\psi_a r_{12}^{-1}\psi_b^*\psi_b dx_1 dx_2$ and $K_{ab} = \int \psi_a^*\psi_b r_{12}^{-1}\psi_b^*\psi_a dx_1 dx_2$

2.4 Basis Set Approximation

The second approximation in HF calculations is due to the fact that the wave function must be described by some mathematical function, which is known exactly for only a few one-electron systems. Because of this approximation, most HF calculation gives a computed energy greater than the Hatree-Fock limit. The one-electron wave function or molecular orbital (MO) can be represented as [26]

$$\psi_i(r) = \sum_{\mu=1}^{2K} c_{\mu i}\phi_\mu(r) \qquad (2.25)$$

The coefficients $c_{\mu i}$ from (Equation 2.25) are known as molecular orbital expansion coefficients. The $\phi_1, \phi_2, \ldots, \phi_{2K}$ are the orthogonal function with known expression. The set of this function is called “basis set”.

The best solution to the approximation of MO could theoretically be obtained by the use of an infinite and complete set of basis functions. The most often used mathematical expressions for the basis functions are the Slater-type orbital (STO) and the Gaussian-type orbitals (GTO).

2.4.1 Slater and Gaussian Type Orbital

Two sorts of basis functions have been widely used.[42] Slater type orbitals(STO), provide reasonable representations of atomic orbitals. However, they are rather difficult to manipulate mathematically. Gaussian type orbitals (GTO) have now largely superseded Slater orbitals. A single Gaussian function does not provide a very good representation of an atomic orbital, but the functions are easy to manipulate because the product of two Gaussians is another Gaussian. Combination of Gaussian can be used to make good approximation to atomic orbitals.

Slater type has the function form

$$\chi_{\zeta,n,l,m}(r,\theta,\varphi) = NY_{l,m}(\theta,\varphi)r^{n-1}e^{-\mathrm{d}\,r} \tag{2.26}$$

N is normalization constant and $Y_{l,m}$ are the spherical harmonic functions. The exponential dependence on the distance between the nucleus and the electron mirrors the exact orbitals for the hydrogen atom. However, STOs do not have any nodes, and nodes in the radical part are introduced by making linear combination of STOs. The exponential dependence ensures a fairly rapid convergence with increasing number of functions. STOs are primarily used for atomic and diatomic systems where high accuracy is required.

Gaussian type orbitals can be written in term of polar or Cartesian coordinates

$$\chi_{\zeta,n,l,m}(r,\theta,\varphi) = NY_{l,m}(\theta,\varphi)r^{(2n-2-1)}e^{-\mathrm{d}\,r^2} \tag{2.27}$$

$$\chi_{\zeta,l_x,l_y,l_z}(x,y,z) = Nx^{l_x}y^{l_y}z^{l_z}e^{-\mathrm{d}\,r^2} \tag{2.28}$$

Where the sum of l_x, l_y and l_z determines the type of orbital (for example $l_x + l_y + l_z = 1$ is a p-orbital).

2.4.2 Classification of Basis Sets

2.4.2.1 Minimal Basis Set

A minimal basis set is a representation that contains just the number of functions that are required to accommodate all the filled orbitals in each atom. In practice, a minimal basis set normally includes all of the atomic orbitals in the shell. Thus, for hydrogen and helium a single s-type function would be required; for elements from lithium to neon the 1s, 2s and 2p functions are used, and so on. The basis sets STO-3G, STO-4G, etc. (in general STO-*n*G), are all minimal basis sets in which *n* Gaussian functions are used to represent each orbital.

The minimal basis sets are well known to have several deficiencies. There are particular problems with compounds containing atoms at the end of a period, such as oxygen or fluorine. Such atoms are described using the same number of basis functions as the atoms at the beginning of the period, despite the fact that they have more electrons. A minimal basis set only contains one function per atomic orbital and as the radial exponents are not allowed to vary during the calculation, the function cannot expand or contract in size in accordance with the molecular environment.

2.4.2.2 Extended Basis Set

The problems with minimal basis sets can be addressed if more than one function is used for each orbital. A basis set which doubles the number of functions in the STO minimal basis set is described as *double zeta* basis (DZ). The double or triple or more of STO minimal basis function allows the linear combination of the ‘contracted’ and the ‘diffuse’ functions which gives an overall result that is intermediate between the two. The basis set coefficient s of the contracted and the diffuse functions are automatically calculates by SCF procedure, which thus automatically determines whether a more

contracted or a more diffuse representation of that particular orbital is required. Such an approach can be providing a solution to the anisotropy problem because it is then possible to have different linear combination for the p_x, p_y and p_z orbitals.

An alternative to the double zeta basis approach is to double the number of functions used to describe the valence electrons but to keep a single function for the inner shells called “split valence double zeta basis”. The rationale for this approach is that the core orbitals do not affect chemical properties very much and vary only slightly from one molecule to another. The most commonly used split valence basis sets are 3-21G, 4-31Gand 6-31G.

2.4.2.3 Polarized Basis Set

The polarization functions describe atomic orbital distortions due to bonding. In molecular system, it is clear that the influence of the other nucleus will distort or polarize the electron density near the nucleus. Simply increasing the number of basis functions (triple zeta, quadruple zeta, etc.) does not necessarily improve the model. In fact, it can give rise to wholly erroneous result, particularly for molecules with strongly anisotropy charge distribution. The use of split valence basis sets can help to surmount the problems with non-isotropic charge distribution but not completely. The charge distribution an atom in a molecule is usually perturbed in comparison with the isolated atom. The distortion can be considered to correspond to mixing p-type character into the 1s orbital of the isolated atom, to give a form of sp hybrid. In a similar manner, the unoccupied d orbitals introduce asymmetry into p orbitals (Figure 2.1). The most common solution to this problem is to introduce polarization function into the basis set. The polarization functions have a higher angular quantum and so correspond to p orbital for hydrogen and d orbitals for the first- and second-row elements.

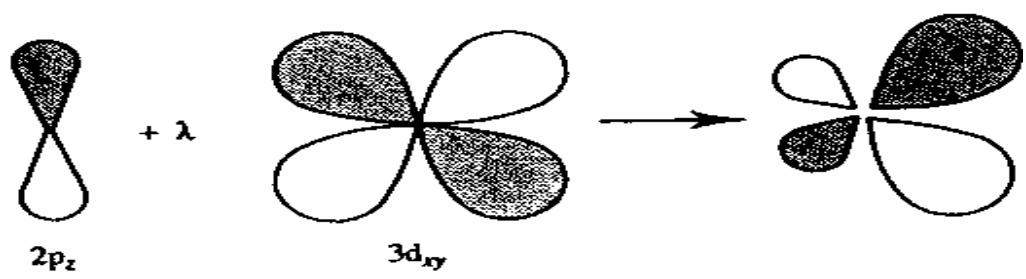

Figure 2.1 The addition of 3dxy orbital to 2pz gives a distorted orbital.

2.4.4 Diffuse Basis Sets

A deficiency of the basis sets is their inability to deal with species such as anions and molecules containing lone pairs which have a significant amount of electron density away from the nuclear centers. This failure arises because the amplitudes of the Gaussian basis functions are rather low far from the nuclei. To remedy this deficiency highly diffuse functions can be added to the basis set. These basis sets are denoted using a '+'; thus the 3-21+G basis set contains an additional single set of diffuse s- and p-type Gaussian functions. '++' indicates that the diffuse functions are included for hydrogen as well as for heavy atoms.

2.5 Density Functional Theory (DFT)

Density functional theory (DFT) has become very popular in recent years. This is justified based on the realistic observation that it is less computationally intensive than other methods with similar accuracy.

2.5.1 The Hohenberg – Kohn Theorem

The starting point of DFT was introduced by Hohenberg and Kohn in 1964, who

showed that the ground-state energy and other properties of a system were uniquely defined by the electron density. They provided two fundamental theorems, which stated as follows:

1) The first Hohenberg – Kohn theorem

The first Hohenberg – Kohn theorem states that the external potential, $V_{Ne}(\vec{r})$, is a unique functional of the electron density $\rho(r)$

$$V_{ext}(\vec{r}) \Rightarrow \rho(\vec{r}) \tag{2.29}$$

And the specification of the ground state densities, $\rho(r)$ are determined the external potential $V_{ext}(\vec{r})$ uniquely,

$$\rho(\vec{r}) \Rightarrow V_{ext}(\vec{r}) \tag{2.30}$$

The first Hohenberg – Kohn theorem; suppose that there are two different external potentials $V_{ext}(r)$ and $V_{ext}(r)'$ which differ more than a constant and each giving the same density, $\rho(r)$ for its ground state. Both different external potentials lead to different Hamiltonians H and H', with two different ground state wave functions Ψ and Ψ'

$$H = H_0 + V_{ext} \quad ; \quad H\Psi = E\Psi \tag{2.31}$$

$$H' = H_0 + V'_{ext} \quad ; \quad H'\Psi' = E\Psi' \tag{2.32}$$

Where Ψ and Ψ' are different N particle wave function and using the variational principle can write the inequality,

$$E_0 = \langle \Psi | H | \Psi \rangle < \langle \Psi' | H | \Psi' \rangle = \langle \Psi' | H' | \Psi' \rangle + \langle \Psi' | H - H' | \Psi' \rangle \tag{2.33}$$

and,

$$E_0' = \langle \Psi' | H' | \Psi' \rangle < \langle \Psi | H' | \Psi \rangle = \langle \Psi | H | \Psi \rangle + \langle \Psi | H' - H | \Psi \rangle \quad (2.34)$$

$$E_0 = E_0' + \int \rho(r)[V_{ext}(r) - V_{ext}(r)']dr \quad (2.35)$$

or,

$$E_0' = E_0 - \int \rho(r)[V_{ext}(r) - V_{ext}(r)']dr \quad (2.36)$$

Adding eq.(2.31) and eq.(2.32) obtain the contradiction

$$E_0 + E_0' < E_0' + E_0 \quad (2.37)$$

where the assumption that the ground-stat densities associated with Ψ and Ψ' were the same permits us to eliminate the integrals as they must sum to zero. However, the sum of the two energies is less than it which must indicated that initial assumption was incorrect. So, the non-degenerate ground-state density must determine the external potential, the Hamiltonian, wave function. [27] It is concluded that there cannot be two different external potentials $V_{ext}(r)$ and $V_{ext}(r)'$ that give the same density $\rho(r)$ for their ground states.

Since the complete ground state energy E_0 is a unique functional of the density $\rho(r)$, so must be its individual parts.

$$E[\rho] = T[\rho] + V_{ext}[\rho] + V_{ee}[\rho]$$

$$= \int \rho(r) V_{ext}(r) dr + F_{HK}[\rho] \quad (2.38)$$

The first term arises from the interaction of the electrons with an external potential $V_{ext}(r)$ (typically due to the Coulomb interaction with the nuclei). $F_{HK}[\rho]$ is the sum of

kinetic energy of the electrons and the contribution from interelectronic interaction. This system independent part, called the Hohenberg – Kohn functional, which is independent of N, R_A and Z_A.

$$F_{HK}[\rho] = T[\rho] + V_{ee}[\rho] \tag{2.39}$$

2) The second Hohenberg – Kohn theorem

The second Hohenberg – Kohn theorem is the variational principle formulated for densities, it can state that

$$E_0 \le E[\tilde{\rho}] = T[\tilde{\rho}] + V_{Ne}[\tilde{\rho}] + V_{ee}[\tilde{\rho}]$$

$$= \int \tilde{\rho}(r) V_{Ne}(r) dr + F_{HK}[\tilde{\rho}] \tag{2.40}$$

where $E[\tilde{\rho}]$ is the energy functional of eq.(2.36) and the equal sign only valid if $\tilde{\rho} = \rho$. So, in principle, it can keep choosing different densities and those that provide lower energies, as calculated by Eq. (2.40), are closer to correct.

Now, the Hohenberg – Kohn functional, $F_{HK}[\rho]$, are still unknown. So it can not make use of the Hohenberg – Kohn theorems to calculate the molecular properties.

2.5.2 The Kohn – Sham Theorem

Kohn and Sham (1965) realized that things would be considerable simpler if only the Hamiltonian operator were one for a non-interacting system of electrons. Such Hamiltonian can be expressed as a sum of one-electron operators. To approximate the Hohenberg – Kohn functional, $F_{HK}[\rho]$, one can easily rederive from the Thomas – Fermi approximation,

$$F_{HK}[\rho] = T[\rho] + V_{ee}[\rho] \tag{2.41}$$

The kinetic energy functional, $T[\rho]$ is split into two parts,

$$T[\rho] = -\frac{1}{2}\nabla^2 + T_C[\rho] = T_S[\rho] + T_C[\rho] \tag{2.42}$$

where the first part $T_s[\rho]$ will be expressed in a one particle approach similar to Hartree – Fock and the second part $T_C[\rho]$ still unknown which contains the difference between the total kinetic energy functional $T[\rho]$ and the one particle term $T_s[\rho]$and the potential energy functional can be written as

$$V_{ee}[\rho] = \frac{1}{2}\iint \frac{\rho(r_1)\rho(r_2)}{|r_1 + r_2|} dr_1 dr_2 + E_{ee}[\rho] = J[\rho] + E_{ee}[\rho] \tag{2.43}$$

The Hohenberg Kohn functional can be written as

$$F_{HK}[\rho] = T_S[\rho] + T_C[\rho] + J[\rho] + E_{ee}[\rho]$$

$$= T_S[\rho] + J[\rho] + E_{XC}[\rho] \tag{2.44}$$

where $T_s[\rho]$ is the kinetic energy, $J[\rho]$ is the electron-electron Coulombic energy, and $E_{XC}[\rho]$ is the exchange correlation functional which still unknown.

The complete energy functional can be written as

$$E[\rho] = T_S[\rho] + J[\rho] + E_{XC}[\rho] + \int \rho(r) V_{Ne}(r) dr \tag{2.45}$$

Similar as in Hartree – Fock theory, the variational principle is applied, which lead finally to the self – consistent Kohn – Sham equations.

$$\hat{f}^{KS}\varphi_i = \varepsilon_i\varphi_i \tag{2.46}$$

where the Kohn – Sham (KS) operator is defined as

$$\hat{f}^{KS} = -\frac{1}{2} + \int \frac{\rho(r_2)}{r_{12}} dr_2 + V_{XC}[\rho] + \sum_A \frac{Z_A}{r_{1A}} \tag{2.47}$$

and

$$V_{XC} = \frac{\delta E_{xc}}{\delta \rho} \tag{2.48}$$

V_{XC} is so-called functional derivative. A functional derivative is analogous in spirit to more typical derivatives, and V_{XC} is perhaps best described as the one-electron operator for which the expectation value of the KS Slater determinant is E_{xc}.

The major problem in DFT is deriving numerically suitable formulas for the exchange – correlation functional. Using the same algorithms as in Hartree – Fock theory, including the usage of basis functions and the self-consistent field (SCF) approach can solve The Kohn – Sham equation. However, the Kohn – Sham orbitals (φ_i) are not the same as the HF orbitals (φ_i^{HF}), which implies that they also lack the physical interpretation of the HF one electron molecular orbitals.

The Kohn-Sham methodology has many similarities, and a few important differences, to the HF approach.

2.5.3 Local Density Methods

The Local Density approximation (LDA) is assumed that the density locally can be treated as a uniform electron gas, or equivalently that the density is a slowly varying function. The exchange energy for a uniform electron gas is given by the dirac formula (Equation (2.49)).

Early attempts deducing functional for the kinetic and exchange energies considered a non-interacting uniform electron gas. For such a system it may be shown that kinetic energies, $T[\rho]$ and exchange energies $K[\rho]$ are given as

$$T_{TF}[\rho] = C_F \int \rho^{5/3}(r)dr$$

$$K_D[\rho] = -C_x \int \rho^{4/3}(r)dr$$

$$C_F = \frac{3}{10}\left(3\pi^2\right)^{2/3} \qquad (2.49)$$

$$C_x = \frac{3}{4}\left(\frac{3}{\pi}\right)^{1/3}$$

For closed-shell systems, the local spin density approximation (LSDA) is equal to LDA and LDA is often used interchangeably with LSDA, although this is not true in the general case (Equation (2.50) and (2.51)).

$$E_x^{LDA}[\rho] = -C_x \int \rho^{4/3}(r)dr$$

$$\varepsilon_x^{LDA}[\rho] = -C_x \rho^{1/3} \qquad (2.50)$$

and

$$E_x^{LSDA}[\rho] = -2^{1/3} C_x \int \left[\rho_\alpha^{4/3} + \rho_\beta^{4/3}\right]dr$$

$$\varepsilon_x^{LSDA}[\rho] = -2^{1/3} C_x \left[\rho_\alpha^{1/3} + \rho_\beta^{1/3}\right] \qquad (2.51)$$

In general case, where the α and β densities are not equal, LDA (Where the sum of the α and β densities is raised to the 4/3 power) has been virtually abandoned and replaced by the LSDA (Equation (2.51)).

LSDA may also be written in terms of the total density and the spin polarization.

$$\varepsilon_x^{LSDA}[\rho] = -\frac{1}{2} C_x \rho^{1/3}\left[(1+\zeta)^{4/3} + (1-\zeta)^{4/3}\right] \qquad (2.52)$$

The X_∞ method proposed by Slater can be considered as an LDA method where the correlation energy is neglected and the exchange term is given as

$$\varepsilon_{X_\alpha}[\rho] = -\frac{3}{2}\alpha C_x \rho^{1/3} \tag{2.53}$$

With $\alpha = 2/3$ this is identical to the dirac expression. The original X_∞ method used $\alpha = 1$, but a value of 3/4 has been shown to give better agreement for atomic and molecular systems.

The correlation energy of a uniform electron gas has been determined by Monte Carlo methods for a number of different densities. In order to use these results in DFT calculations, it is desirable to have a suitable analytic interpolation formula. This has been constructed by Vosko, Wilk and Nusair (VWN) and is in general considered to be a very accurate fit. It is interpolate between the unpolarized ($\zeta = 0$) and spin polarized ($\zeta = 1$) limits by the following functional. [28]

$$\varepsilon_c^{VWN}(r_s,\zeta) = \varepsilon_c(r_S,0) + \varepsilon_a(r_S)\left[\frac{f(\zeta)}{f''(0)}\right]\left[1-\zeta^4\right] + \left[\varepsilon_c(r_S,1) - \varepsilon_c(r_S,0)\right] f(\zeta)\zeta^4$$

$$f(\zeta) = \frac{(1+\zeta)^{4/3} + (1-\zeta)^{4/3} - 2}{2\left(2^{1/3}-1\right)} \tag{2.54}$$

The $\varepsilon_c(r_S,\zeta)$ and $\varepsilon_a(r_S)$ functionals are parameterized as

$$\varepsilon_{c/a}(x) = A\left\{\ln\frac{x^2}{X(x)} + \frac{2b}{Q}\tan^{-1}\left(\frac{Q}{2x+b}\right) - \frac{bx_0}{X(x_0)}\left[\ln\frac{(x-x_0)2}{X(x)} + \frac{2(b+2x_0)}{Q}\tan^{-1}\left(\frac{Q}{2x+b}\right)\right]\right\} \tag{2.55}$$

$$x = \sqrt{r_S}$$

$$X(x) = x^2 + bx + c$$

$$Q = \sqrt{4c - b^2}$$

The parameters *A*, x_0, *b* and *c* are fitting constants, different for $\varepsilon_c(r_S,0)$, $\varepsilon_c(r_S,1)$ and $\varepsilon_a(r_S)$.

A modified form for $\varepsilon_{c/a}(r_S)$ has been give by Perdew and Wang, and is used in connection with the PW91 functional.

$$\varepsilon_{c/a}^{PW91} = -2a\rho(1+\alpha x^2)\ln(1+\frac{1}{2\alpha(\beta_1 x+\beta_2 x^2+\beta_3 x^3+\beta_4 x^4)} \qquad (2.56)$$

Here *a*, α, β_1, β_2, β_3 *and* β_4 are suitable constants.

In general, the LSDA approximation is underestimates the exchange energy by ~10%. Electron correlation and bond strengths are overestimated. The fundamental assumptions of LSDA methods are often found to provide results with accuracy similar to that obtained by HF methods.

2.5.4 Gradient Corrected Approximation

Improvement over the LSDA approach has to consider a non-uniform electron gas. A step in this direction makes the exchange and correlation energies dependent not only on the electron density, but also on derivatives of the density. Such methods are known as Gradient correct or generalized gradient approximation (GGA) methods. GGA methods are also sometime referred to as non-local methods. [29]

Perdew and Wang (PW86) proposed modifying the LSDA exchange expression to that shown in Equation (2.57). Where x is a dimensionless gradient variable, and a, b and c are suitable constants.

$$\varepsilon_x^{PW86} = \varepsilon_x^{LDA}\left(1+ax^2+bx^4+cx^6\right)^{1/15} \qquad (2.57)$$

$$x = \frac{\left|\nabla_\rho\right|}{\rho^{4/3}}$$

Becke proposed a correlation (B or B88) to the LSDA exchange energy.

$$\varepsilon_x^{B88} = \varepsilon_x^{LDA} + \Delta\varepsilon_x^{B88}$$

$$\Delta\varepsilon_x^{B88} = -\beta\rho^{1/3}\frac{x^2}{1+6\beta\sinh^{-1}x} \tag{2.58}$$

The β parameter is determined by fitting to known atomic data and x defined in Equation (2.57)

Perdew and Wang (PW91) have proposed an exchange functional similar to B88, to be used in connection with the PW91 correlation functional given below.

$$\varepsilon_x^{PW91} = \varepsilon_x^{LDA}\left(\frac{1+xa_1\sinh^{-1}(xa_2)+(a_3+a_4e^{-bx^2})x^2}{1+xa_1\sinh^{-1}(xa_2)+a_5x^2}\right) \tag{2.59}$$

where $a_{1\text{-}5}$ and b are suitable constants and x is defined in Equation (2.57).

There have been various gradient corrected functional forms proposed for the correlation energy. One popular functional (not a correlation) is due to Lee, Yang and Parr (LYP) and has the form,

$$\varepsilon_c^{LYP} = -a\frac{\gamma}{(1+d\rho^{1/3})} - ab\frac{\gamma e^{-c\rho^{-1/3}}}{9(1+d\rho^{-1/3})\rho^{8/3}}\times\left[\begin{array}{l}18(2^{2/3})C_F(\rho_\alpha^{8/3}+\rho_\alpha^{8/3})-18\rho t_w \\ +\rho_\alpha(2t_w^\alpha+\nabla^2\rho_\alpha)+\rho_\beta(2t_w^\beta+\nabla^2\rho_\beta)\end{array}\right] \tag{2.60}$$

$$\gamma = 2\left[1-\frac{\rho_\alpha^2+\rho_\beta^2}{\rho^2}\right]$$

$$t_w^\sigma = \frac{1}{8}\left(\frac{|\nabla\rho_\sigma|^2}{\rho_\sigma}\right)-\nabla^2\rho_\sigma$$

where the *a, b, c* and *d* parameters are determined by fitting to data for the helium atom and the t_W functional is the local Weizsacker kinetic energy density.

This functional was later modified to the following form (also a correction to the LSDA energy) by Perdew and Wang in 1991 (PW91 or P91).

$$\Delta\varepsilon_c^{PW91}[\rho] = \rho(H_0(t,r_S,\zeta)+H_1(t,r_S,\zeta))$$

$$H_0(t,r_S,\zeta) = b^{-1} f(\zeta)^3 \ln\left[1 + a\frac{t^2 + At^4}{1 + At^2 + A^2t^4}\right]$$

$$H_1(t,r_S,\zeta) = \left(\frac{16}{\pi}\right)\left(3\pi^2\right)^{1/3}\left[C(\rho) - c\right] f(\zeta)^3 t^2 e^{-dx^2/f(\zeta)^2}$$

$$f(\zeta) = \frac{1}{2}\left((1+\zeta)^{2/3} + (1-\zeta)^{2/3}\right) \qquad (2.61)$$

$$t = \left(\frac{192}{\pi^2}\right)^{1/6} \frac{|\nabla\rho|}{2 f(\zeta)\rho^{7/6}}$$

$$A = a\left[e^{-b\varepsilon_c(r_S,\zeta)/f(\zeta)^3} - 1\right]^{-1}$$

$$C(\rho) = \ell_1 + \frac{\ell_2 + \ell_3 r_S + \ell_4 r_S^2}{1 + \ell_5 r_S + \ell_6 r_S^2 + \ell_7 r_S^3}$$

where $\varepsilon(r_S,\zeta)$ is the PW92 parameterization of the LSDA correlation energy functional (Equation 2.56), and *a, b, c* and *d* are suitable constants.

It has several functionals violate fundamental restrictions, such as predicting correlation energies for one-electron systems (for P86 and PW91). One of functionals which does not have these problems is due to Becke, which has the form

$$\varepsilon_c^{B95} = \varepsilon_c^{\alpha\beta} + \varepsilon_c^{\alpha\alpha} + \varepsilon_c^{\beta\beta}$$

$$\varepsilon_c^{\alpha\beta} = \left[1 + a\left(x_\alpha^2 + x_\beta^2\right)\right]^{-1} \varepsilon_c^{PW91,\alpha\beta}$$

$$\varepsilon_c^{\sigma\sigma} = \left[1 + bx_\sigma^2\right]^{-2} \frac{D_\sigma}{D_\sigma^{LDA}} \varepsilon_c^{PW91,\sigma\sigma} \qquad (2.62)$$

$$D_\sigma^{LDA} = 2^{5/3} C_F \rho_\sigma^{5/3}$$

$$D_\sigma = \sum_i^N |\nabla\varphi_i|^2 - \frac{(\nabla\rho_\sigma)^2}{4\rho_\sigma} \qquad x = \frac{|\nabla_\rho|}{\rho^{4/3}}$$

Here σ run over α or β spins, a and b are fitting parameters, and ε_c^{PW91} is the Perdew – Wang parameterization of the LSDA correlation functional (Equation (2.56)).

2.5.5 Hybrid Methods

From the Halmiltonian and the definition of the exchange-correlation energy, an exact connection can be made between the exchanger-correlation energy and the corresponding potential connection the non-interacting reference and the actual system. The resulting equation is called the Adiabatic Connection Formula (ACF) and involves integration over the parameters λ which "turn on" the electron-electron interaction.

$$E_{xc} = \int_0^1 \langle \Psi_\lambda | V_{xc}(\lambda) | \Psi_\lambda \rangle dr \tag{2.63}$$

In the crudest approximation (taking V_{XC} to be linear in λ) the integral is given as the average of the values at the two end-points.

$$E_{xc} \approx \frac{1}{2}\langle \Psi_0 | V_{xc}(0) | \Psi_0 \rangle + \frac{1}{2}\langle \Psi_1 | V_{xc}(1) | \Psi_1 \rangle \tag{2.64}$$

Since the exact wave function in this case is a single Slater determinant composed of Kohn-Sham (KS) orbitals, the exchange energy is exactly that given by HF theory. If the KS orbitals are identical to the HF orbitals, the "exact" exchange is precisely the exchange energy calculated by HF wave mechanics methods. The last term in eq. (2.64) is still unknown. Approximating it by the LSDA result defines the Half-and Half (H+H) method.

$$E_{xc}^{H+H} = \frac{1}{2}E_x^{exact} + \frac{1}{2}\left(E_x^{LSDA} + E_c^{LDSA}\right) \tag{2.65}$$

Since the GGA method give a substantial improvement over LDA, generalized version of the Half-and-Half method may be defined by writing the exchange energy as a suitable combination of LSDA, exact exchange and gradient correlation term. The correlation energy may similarly be taken as the LSDA formula plus a gradient correlation term.

$$E_{xc}^{B3PW91} = (1-a)E_x^{LSDA} + aE_x^{exact} + bE_x^{B88} + E_c^{LSDA} + cE_c^{GGA} \tag{2.66}$$

Models which include exact exchange are often called hybrid methods, the name adiabatic connection model (ACM) and Beck 3 parameter functional (B3) are example of such hybrid models defined by eq. (2.66). The typical values of parameters a, b and c are 0.20, 0.72 and 0.81, respectively. Owing to the substantially better performance of such parameterized functionals the Half-and-Half model is rarely used anymore. The B3 procedure has been generalized to include more fitting parameters, the improvement is rather small.

Subsequently, Stevens et al. (1994) modified this functional to use LYP instead of PW91. Because LYP is designed to compute the full correlation energy, and not a correlation to LSDA, the B3LYP model is defined by

$$E_{xc}^{B3LYP} = (1-a)E_x^{LSDA} + aE_x^{HF} + bE_x^{B} + E_c^{LSDA} + cE_c^{LYP} \tag{2.67}$$

where *a, b* and *c* have the same value as in B3PW91. Of all modern functionals, B3LYP has proven the most popular to date.

2.6 Molecular Dynamic Simulations

Molecular dynamic (MD) simulations is a computational technique regularly used in condensed matter physics, chemistry, and related fields. MD is a simulation of the time-dependent behavior of molecular system. It requires a way to compute the energy of the system, most often using a molecular mechanics calculation. This energy expression

In molecular dynamics, successive configurations of the system are generated by integrating Newton's laws of motion. The result is a trajectory that specifies how the positions and velocities of the particles in the system vary with time. The trajectory is obtained by solving the differential equations embodied in Newton's second law (F=ma).

MD methods solve Newton's equation of motion for atoms on an energy surface. The available energy for the molecule is distributed between potential and kinetic energy, and molecules are overcome barriers separating minima if the barrier height is less than the total energy minus the potential energy. Given a high enough energy, which is closely related to the simulation temperature, the dynamics will sample the whole surface, but this will also required an impractically long simulation time. Since quite small time steps must be used for integrating Newton's equation, the simulation time is short (pico- or nanoseconds). Combined with the use of "reasonable" temperatures (few hundreds or thousands of degrees), this means that only the local area around the starting point is sampled, and that only relatively small barriers (few kcal/mol) can be overcome. Different (local) minima may be generated by selecting configurations at intervals during the simulation and subsequently minimizing these structures. [30]

The steps in a molecular dynamics simulation of an equilibrium system are as follow

1 Choose initial position for the atoms. For a molecule, this is whatever geometry is available, not necessarily an optimized geometry. For liquid simulations, the molecules are often started out on a lattice. For solvent solute systems, the solute is often placed in the center of a collection of solvent molecules, with positions obtained from a simulation of the neat solvent.

2 Choose an initial set of atom velocities. These are usually chosen to obey Boltzmann distribution for some temperature, and then normalized so that the net momentum for the entire system is zero.

3 Compute the momentum of each atom from its velocity and mass.

4 Compute the forces on each atom from the energy expression. This is usually molecular mechanics force field designed to be used in dynamic simulations.

5 Compute new positions for the atoms a short time later, called the time step. This is numerical integration of Newton's equations of motion using the information obtained in the previous steps.

6 Compute new velocities and accelerations for atoms.

7 Repeat steps 3 through 6.

8 Repeat this iteration long enough for the system to reach equilibrium. In this case, equilibrium is not the lowest energy configuration; it is configuration that is reasonable for the system with the given amount of energy.

9 Once the system has reached equilibrium, begin saving the atomic coordinates every few iterations. This information is typically saved every 5 to 25 iterations. This list of coordinates over time is called a trajectory.

10 Continue iterating and saving data until enough data have been collected to give results with the desired accuracy.

11 Analyze the trajectories to obtain information about the system. This might be determined by computing radial distribution functions, diffusion coefficients, vibrational motions, or any property computable from this information.

2.6.1 Parameters of Molecular dynamics

A molecular dynamic simulation needs

1) A Starting Structure

Molecular dynamic simulations must begin with a sensible geometry for the structure of interest, and this may be difficult to obtain. Typically, an approximate model will be built using any experimental data that are available, maybe crystal structure data, and this will then be minimized (almost certainly to a local minimum rather than the global minimum) so that all the bond lengths and bond angles have sensible values. It is not necessary to start with the global minimum, or even a structure close to the global minimum, but if the starting structure is too strained, errors in the MD simulations may accumulate too rapidly, and the structure may 'blow up'.

2) Temperature and Energy

The amount of energy the structure is given depends on the temperature of the system. The energy is divided between movement and potential energy, just as a ball on a spring will be moving quickly when the spring is relaxed and stationary when the spring is fully compressed or fully extended.

The energy is divided between the atoms so that each atom gets more or less the same energy. If all the energy were given to one atom, then that atom would probably escape from the molecule, and this is not a situation that force field are good coping with.

Errors in the calculation mean that it is necessary to check the energy after every step, and adjust it so that the system does not get carried away. This is due both to the errors in the numerical solutions of Newton's equations, and to the inability of force fields to predict the properties of much distorted structures.

3) Step Size

The calculation of how the molecule will move works by calculating what the molecule will be doing a very short time in the future. This short time has to be much shorter than the shortest time in which anything interesting can be happen to the molecule. One of the problems with solving coupled differential equations is finding out how short a time is necessary. This is called the characteristic time for the system. The fastest thing

can happen to a molecule is an electronic transition. However, molecular mechanics ignores electrons, so these need not be considered. The fastest mechanical change to a molecule is the property which determines the characteristic time.

The characteristic time for a molecular dynamic simulation may be estimated by considering an ordinary infra red spectrum. The shortest period of oscillation in an infra red spectrum is about ten femtoseconds (about $3300cm^{-1}$). The time step usually chosen for molecular dynamics is one femtosecond ($33,000cm^{-1}$).

This mean the molecular dynamics run calculates many structures for each oscillation of a carbon-hydrogen bond, and very many structures for the slower movements in the molecule. There are various tricks that can be used to speed things up. For example, the fastest thing in molecular dynamic simulations is the vibrational of bonds to hydrogen. It is possible to constrain the carbon-hydrogen bond lengths, on the grounds that this is unlikely to affect the movement of the structure very much. This turns out to be a reasonable approximation, and as a result of the calculation runs faster. And it is possible to use a slightly larger time step, perhaps two femtoseconds instead of one. It would be useful to constrain bond angles in the same away, but this does not work so well because it seriously inhibits torsional rotations.

4) Length of a Simulation

Usually a simulation would be desirable to run it for longer than is feasible, but the choice of a termination time will depend on the information required. A simulation might only last for about ten picoseconds. A simulation of few picoseconds will take hours of computer time. The first of molecular dynamic simulations of a macromolecule was carried out in 1977, by McCammon, Gelim and Karplus. By 1990, computers had become so much more powerful that Karplus and Petsko could comment that for many problems 100 ps simulations were sufficient, and this is reasonable length of time to run a simulation. However 100 ps is a very short time indeed.

A molecular dynamic simulation takes a while to settle down. It begins with random components of energy, and these slowly distribute themselves s around the molecule. At the beginning of run, the energy tends to fluctuate over a large range and

then the range decreases as the run proceeds. The time required for the simulation to settle down depends on the molecule and on the choice of the starting structure. If the starting structure was very strained, it may be long time before the molecule settle down, where if the starting structure was the only significantly minimum of a structure then the simulation may produce consistent energies almost immediately.

2.6.2 Setting up and Running Molecular Dynamic Simulations

Performing MD simulations are in the microcanonical ensemble. It is necessary to establish an initial configuration of the system. The initial configuration may be obtained from experimental data, from a theoretical model or from a combination of two. It's also necessary to assign initial velocities to the atoms. This can be done by randomly selecting from a Maxwell-Boltzmann distribution at the temperature of interest:

$$p(v_{ix}) = \left(\frac{m_i}{2\pi k_B T}\right)^{1/2} \exp\left[-\frac{1}{2}\frac{m_i v_{ix}^2}{k_B T}\right] \qquad (2.68)$$

The Maxwell-Boltzmann equation provides the probability that an atom *i* of mass m_i has a velocity v_{ix} in the *x* direction at a temperature T. A Maxwell-Boltzmann equation is a Gaussian distribution, which can be obtained using a random number generator. Most random number generators are in the range 0 to 1.

The initial velocities are often adjusted so that the total momentum of the system is zero. Such a system then samples from the constant *VNE*P ensemble. Having set up the system and assigned the initial velocities. At each step the force on each atom must be calculated by differentiating the potential function. The force on an atom may contributions from the various terms in the force field such as bonds, angles, torsional terms and non-bonded interactions.

The first stage of the MD simulations is the equilibration phase, the purpose of which is to bring the system to equilibrium from the starting configuration. During

equilibration steps, various parameters are monitored together with the actual configurations. When these parameters achieve stable values then the production phase can commence. It is during the production phase that thermodynamic properties and other data are calculated. The parameters that are used to characterize whether equilibrium has been reached depend to some extent on the system being simulated but invariably include the kinetic, potential and total energies, the velocities, the temperature and the pressure. The kinetic and potential energies would be expected to fluctuate in a simulation in the microcanonical ensemble but the total energy should remain constant.

At the start of the production phase all counter are set to zero and the system is permitted to evolve. In a microcanonical ensemble no velocity scaling is performed during the production phase and so the temperature becomes a calculated property of the system. Various properties are routinely calculated and stored during the production phase for subsequent analysis and processing. Careful monitoring of these properties during the simulation can show whether the simulation is ‘well behaved’ or not. It may be to restart a simulation if problems are encountered. It is also usual to store the positions, energies and velocities of configurations at regular intervals, from which other properties can be determined once the simulation has finished.

2.6.3 Molecular Dynamic at Constant Temperature and Pressure

Molecular dynamics is traditionally performed in the constant *NVE* (or *NVE*P) ensemble. Although thermodynamic results can be transformed between ensembles, this is strictly only possible in the limit of infinite system size. It may be desired to perform the simulation in a different ensemble. The two most common alternative ensembles are the constant NVT and NPT ensembles.

1) Constant Temperature Dynamics

There are several reasons why we might want to maintain control the temperature during a molecular dynamics simulation. Even in a constant NVE simulation it is common practice to adjust the temperature to the desired value during the equilibration phase. A constant temperature simulation may be required if the behavior of the system changes with temperature.

The change in temperature between successive time steps is:

$$\Delta T = \frac{\delta t}{\tau}\left(T_{bath} - T(t)\right) \tag{2.69}$$

τ is a coupling parameter whose magnitude determines how tightly the bath and the system are coupled together.

The scaling factor for the velocities is thus:

$$\lambda^2 = 1 + \frac{\delta t}{\tau}\left(\frac{T_{bath}}{T(t)} - 1\right) \tag{2.70}$$

If τ is large, then the coupling will be weak. If τ is small, the coupling will be strong and when the coupling parameter equals the time step ($\tau = \delta t$) then the algorithm is equivalent to the simple velocity scaling method. A coupling constant of approximately 0.4 ps. has been suggested as an appropriate value to use when the time step is 1 fs., giving $\delta t/\tau \approx 0.0025$. The advantage of this approach is that it does permit the system to fluctuate about the desired temperature.

Two methods that do generate rigorous canonical ensembles if properly implemented are the *stochastic collision* method and the *extend system* method.

The mean rate (ν) at which each particle should suffer a stochastic is given by:

$$\nu = \frac{2a\kappa}{3k_B\eta^{1/3}N^{2/3}} \tag{2.71}$$

a is a dimensional constant, κ is the thermal conductivity and η is the number density of the particles.

Extended system methods, originally introduced for performing constant temperature molecular dynamics by Nosé in 1984 and subsequently developed by Hoover in 1985, consider the thermal reservoir to be an integral part of the system. The reservoir is represented by an additional degree of freedom, labeled s. The reservoir has potential energy $(f+1)k_BT \ln s$, where f is the number of degrees of freedom in the physical system and T is the desired temperature. The reservoir also has kinetic energy $(Q/2)(ds/dt)^2$. Q is a parameter with the dimensional of energy × (time)^2 and can be considered the mass of the extra degree of freedom. The magnitude of Q determines the coupling between the reservoir and the real system and so influences the temperature fluctuations.

The parameter Q controls the energy flow between the system and the reservoir. If Q is large then the energy flow is slow and if Q is too small then the energy oscillates. Nosé has suggested that Q should be proportional to fk_BT; the constant of proportionality can then be obtained by performing a series of trial simulations for a test system and observing how well the system maintains the desired temperature.

2) Constant Pressure Dynamics

Wish to specify the temperature in a molecular dynamics simulation, so it may be to desire to maintain the system at a constant pressure. This enables the behaviour of the system to be explored as a function of the pressure. Constant pressure conditions may also be important when the number of particles in the system changes. The pressure often fluctuates much more than quantities such as the total energy in a constant *NVE* molecular dynamics simulation. This is expected because the pressure is related to the virial, which is obtained as the product of the positions and the derivative of the potential energy function.

A macroscopic system maintains constant pressure by changing its volume. A simulation in the isothermal-isobaric ensemble also maintains constant pressure by changing the volume of the simulation cell. The amount of volume fluctuate is related to the isothermal compressibility, κ

$$\kappa = \frac{1}{V}\left(\frac{\partial V}{\partial P}\right)_T \tag{2.72}$$

Many methods used for pressure control are analogous to those used for temperature control. The rate of change of pressure is given by:

$$\frac{dP(t)}{dt} = \frac{1}{\tau_P}\left(P_{bath} - P(t)\right) \tag{2.73}$$

τ_P is the coupling constant, P_{bath} is the pressure of the 'bath', and $P(t)$ is the actual pressure at time t. The volume of the simulation box is scaled by a factor λ, which is equivalent to scaling the atomic coordinates by a factor $\lambda^{1/3}$. Thus:

$$\lambda = 1 - \kappa\frac{\delta t}{\tau_P}\left(P - P_{bath}\right) \tag{2.74}$$

The new positions are given by:

$$r_i^{/} = \lambda^{1/3} r_i \tag{2.75}$$

The extend-system temperature-scaling method of Nosé uses scale time. In the extend pressure method the coordinates of the extended system are related to the 'real' coordinates by:

$$r_i^{/} = V^{-1/3} r_i \tag{2.76}$$

2.6.4 Radial Distribution Functions

Radial distribution functions (RDF) are a useful way to describe the structure of a system, particularly of liquids.[31] Consider a spherical shell of thickness δr at a distance r from a chosen atom (Figure 2.5). The volume of the shell is given by:

$$V = 4\pi r^2 \delta r + 4\pi \delta r^2 + \frac{4}{3}\pi \delta r^3 \approx 4\pi r^2 \delta r \qquad (2.77)$$

The number of particles per unit volume is ρ, then the total number in the shell is $4\pi\rho r^2 \delta r$ and so the number of atoms in the volume element varies as r^2.

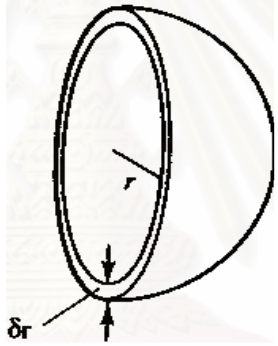

Figure 2.2 Radial distribution functions use a spherical shell of thickness δr.

The pair distribution function, *g(r)*, gives the probability of finding an atom (or molecule, if simulating a molecular fluid) a distance r from another atom (or molecule) compare to the ideal gas distribution. *g(r)* is thus dimensionless. Higher radial distribution functions(e.g. the triplet radial distribution function) can also be defined but are rarely calculated and so references to the 'radial distribution function' are usually taken to mean the pairwise version. In a crystal, the radial distribution function has an infinite number of sharp peaks whose separations and heights are characteristic of the lattice structure.

The RDF calculated from MD simulations of liquid argon (shown in Figure 2.6) is typical. For short distances (less than the atomic diameter) *g(r)* is zero. This is due to the strong repulsive forces. The first (and large) peak occurs at $r \approx 3.7$ Å, with *g(r)* having a

value of about 3. This means that it is three times more likely that two molecules would have this separation than in the ideal gas. The RDF then falls and passed through a minimum value around $r \approx 5.4$ Å. The chances of finding two atoms with this separation are less than for the ideal gas. At long distances, *g(r)* tends to the ideal gas value, indicating that there are no long-rang order.

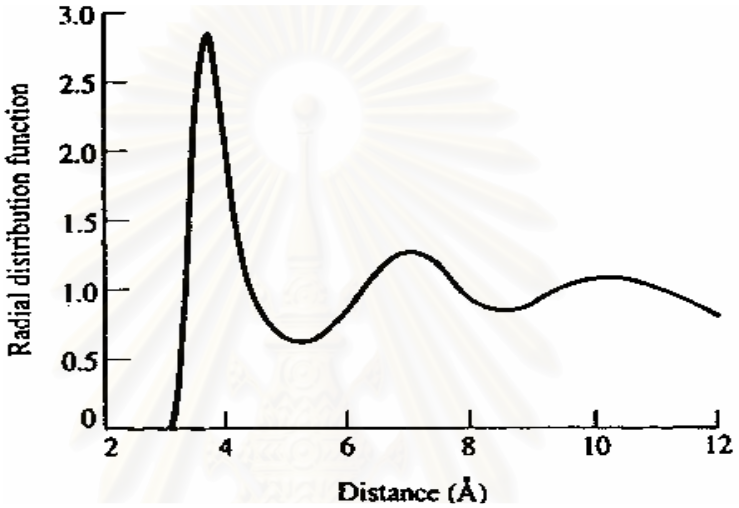

Figure 2.3 Radial distribution functions determined from a 100 ps. molecular dynamic simulations of liquid argon at a temperature of 100 K and a density of 1.396 cm^{-1} and a density of 1.396 g cm^{-3}.

For molecules, the orientation must be taken into account if the true nature of the distribution function for molecules is usually measured between two fixed points. For more complex molecules it is usual to calculate a number of site-site distribution functions.

CHAPTER 3

CALCULATION METHODS

The calculations were carried out as following. First structures of H-ZSM-5 for different Al substitution were generated. These MD simulations were performed to obtain equilibrium geometries for these H-ZSM-5. Finally, cluster model were prepared from the equilibrium structures and quantum calculation were performed to obtain proton affinity (PA) of zeolites.

3.1 HZSM-5 Catalysts

Initial X-ray structures of MFI-framework are taken from the library of Cerius2 program package. The zeolite structure in the database contains only silicon and oxygen atoms (Figure 3.1) and therefore it is necessary to alter the structure to obtain the preferred silicon to aluminum ratio. By replacing Si atom with Al using Crystal Builder in Cerius2 program package, model of H-ZSM-5 with 2 different Si/Al ratios, *i.e.* 47 (disubstituted) and 95 (monosubstituted) were constructed. However, the excess negative charges causing by Si replacement were compensated by adding H+ to O near Si substitutions.

1) Preparation of H-ZSM-5 zeolite structure

There are 12 T-sites for the Si/Al ratio of 95 and 23 T-sites for Si/Al ratio of 47. These T-sites are listed in Tables 3.1 and 3.2, respectively. For the Si/Al ratio of 95 all T-site were considered but only 8 sites *i.e.* T4,T4 , T5,T12 , T6,T12 , T7,T12 (model1) , T7,T12 (model2) , T7,T12 (model3), T8,T8 and T9,T10 were studied for the Si/Al ratio of 47. Only T-sites within the pore of the straight channel are of interest. Figures 3.2 and 3.3 are display position of T-sites for the Si/Al ratios of 95 and 47, respectively. After Al substitutions were performed, the models then were made periodic to mimic solid structures using Crystal Builder program in Cerius2 package.

Table 3.1 The monosubstitution site for the Si/Al ratio of 95.

Model	**Al-site (T-site)**
1	1
2	2
3	3
4	4
5	5
6	6
7	7
8	8
9	9
0	10
11	11
12	12

Table 3.2 The disubstitution site for the Si/Al ratio of 47. [9]

Model	**Al-sites (T-sites)**		**Model**	**Al-sites (T-sites)**	
1	T11	T11	13	T3	T9
2	**T8**	**T8**	**14**	**T6**	**T12**
3	T6	T6	15	T4	T4
4	T5	T5	**16**	**T9**	**T10**
5	T1	T1	17	T7	T12
6	T2	T2	18	T1	T6
7	T3	T3	19	T2	T5
8	T7	T9	20	T4	T10
9	T7	T9	**21**	**T4**	**T4**
10	**T7**	**T12**	22	T9	T12
11	**T7**	**T12**	**23**	**T5**	**T12**
12	**T1**	**T7**			

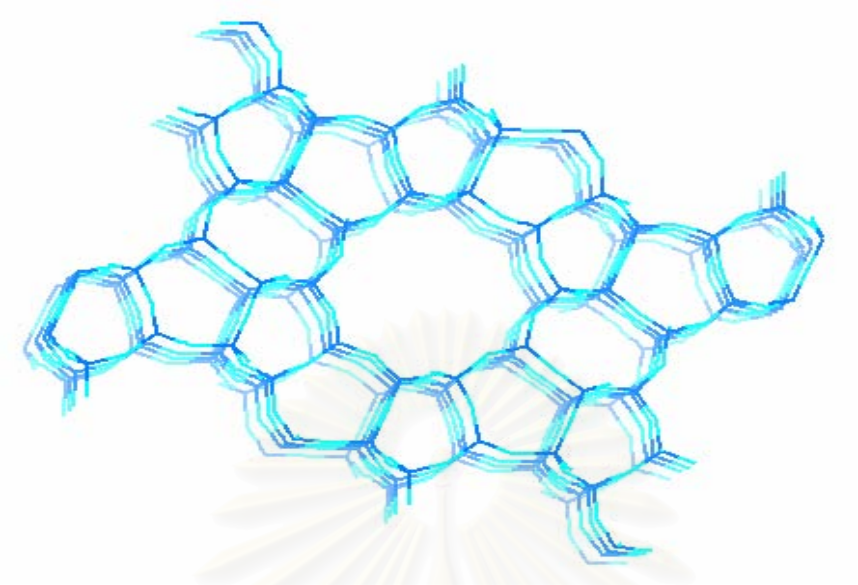

Figure 3.1 The structure of ZSM-5(MFI) zeolite.

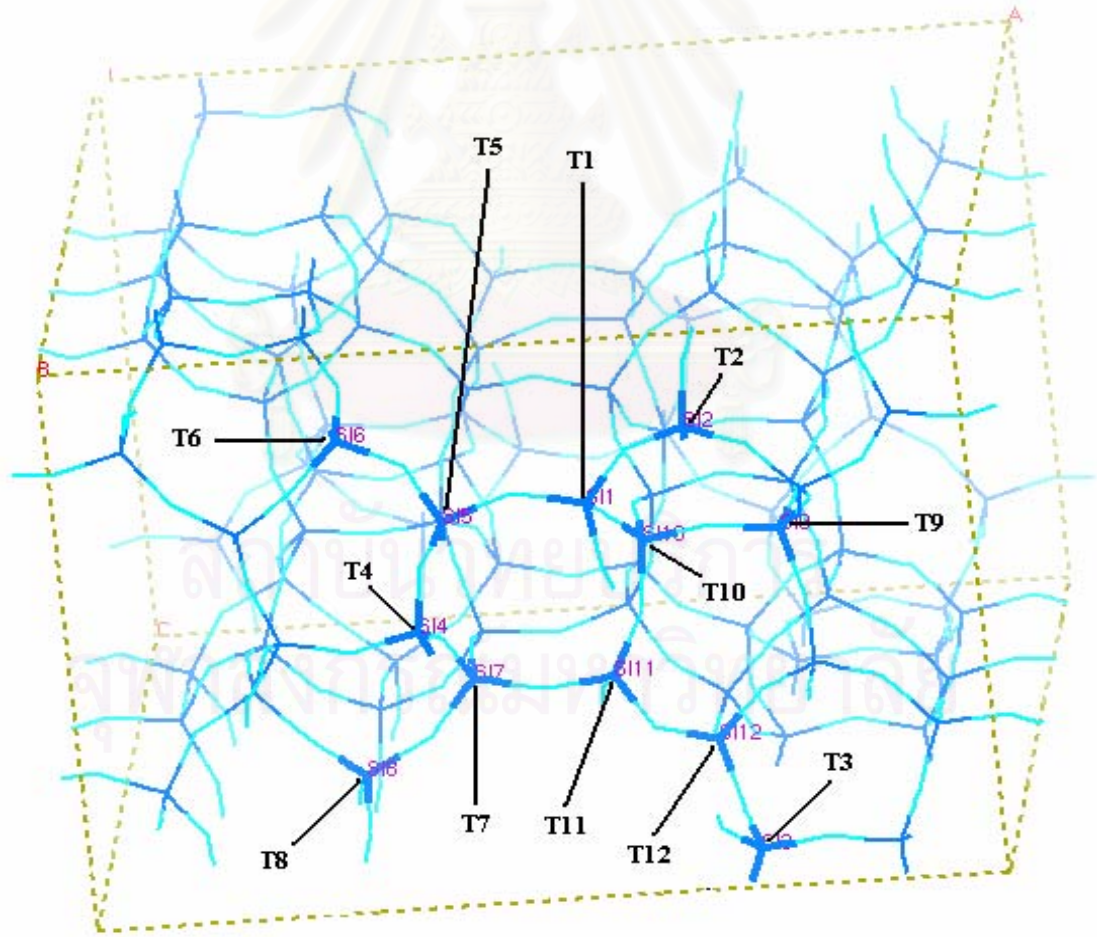

Figure 3.2 The 12 T-sites of structure of ZSM-5 with the Si/Al ratio of 95.

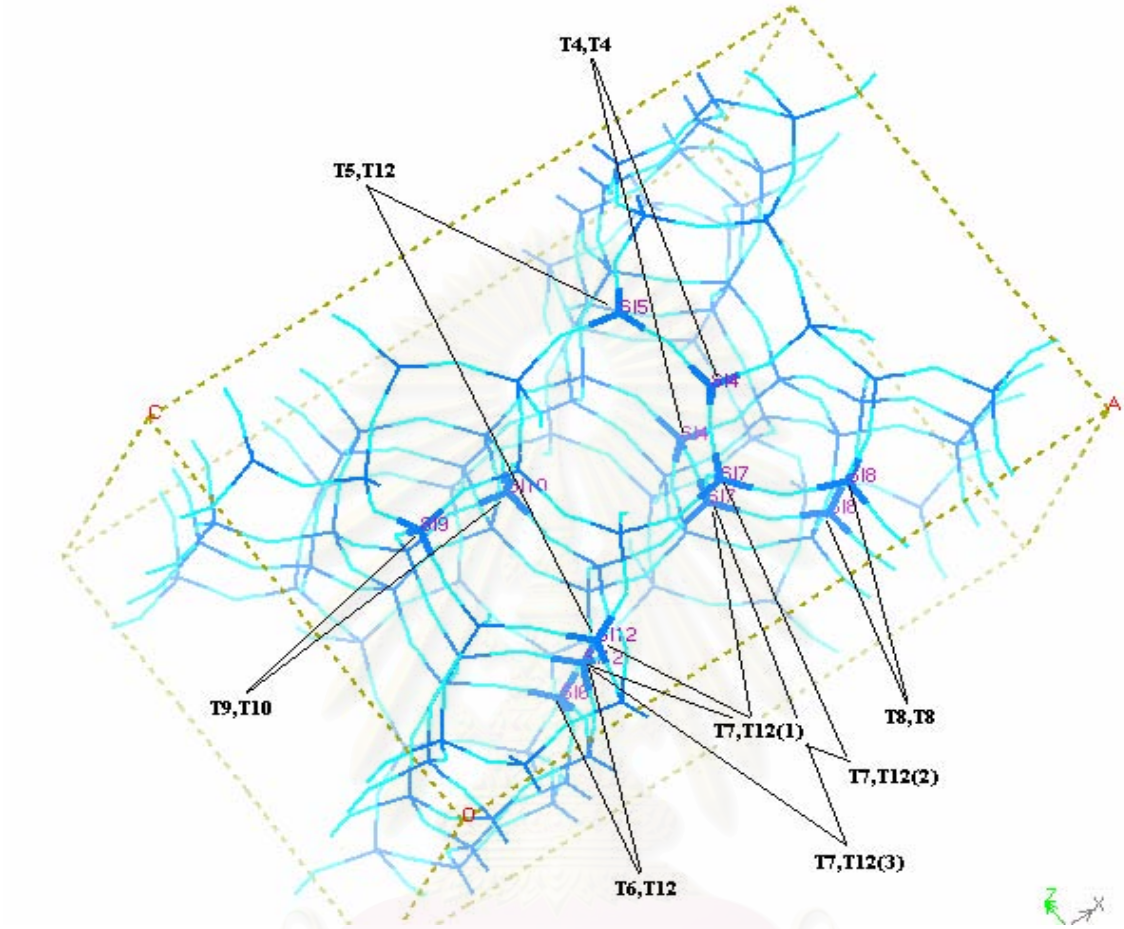

Figure 3.3 The 8 T-sites of ZSM-5 with the Si/Al ratio of 47.

3.2 Molecular Dynamic Simulations

After obtaining H-ZSM-5 structures, the MD simulations were performed in the following manners.

1) Energy minimization

Energy minimizations or geometry optimizations were performed to obtain good starting structure for further MD simulations (due to the size difference between Al and Si, patterns of atoms in ZSM-5 might not be in the proper place after the substitution was made). The energy minimization was performed using CVFF force field.

2) Equilibration

From the structure obtained in energy minimization, the structure is first brought to their equilibrium temperature in the equilibration step. This is done by performing NVT ensemble with total time 10.0 ps and time step of 0.1 fs. The temperature is kept constant at 300 K using Nosé method.

3) Production.

Once the structure reaches the equilibrium temperature, more MD runs are made. This is done using NVT ensemble with 2.0 ns total run time and 0.1 fs time step. Again the temperature is kept constant at 300 K using Nosé method. After MD simulation is completed, analysis such as radial distribution function (RDF) is made.

3.3 Quantum Calculations

To verifying acidity of H-ZSM-5 with different Si/Al ratio and Al substitution, quantum calculations on cluster models of protonated (ZH^+) and unprotonated (Z) zeolites were made. The cluster models were taken from final structures of MD simulations. These were done for ZH^+ by cutting cluster around Al substitutions. The incomplete T-O bonds were then saturated with H, as displayed in Figure 3.4. The TO-H bond distances and T-O-H bond angles were determined by performing partial optimization while keeping positions of other atoms fixed. The partial optimization of TO-H bond distances and T-O-H bond angles were obtained from thesis of Miss Kanjarut Sukrat.[43] That study reported TO-H bond distances of 0.96 Å and T-O-H bond angles of 116.0 degree. For Z, the structures were prepared by deleting H^+ in ZH^+ and single point energy calculations were carried out from these structures. All calculations were carried out using B3LYP/6-31G (d, p) with Gaussian98 program. From energies of protonated and unprotonated

zeolites, the proton affinities of ZSM-5 with different Si/Al ratio and Al substitutions can be calculated according to

$$Z + H^+ \longrightarrow ZH^+$$

$$\text{Proton affinity (PA)} = [E(Z) - E(ZH^+)] \quad (3.1).$$

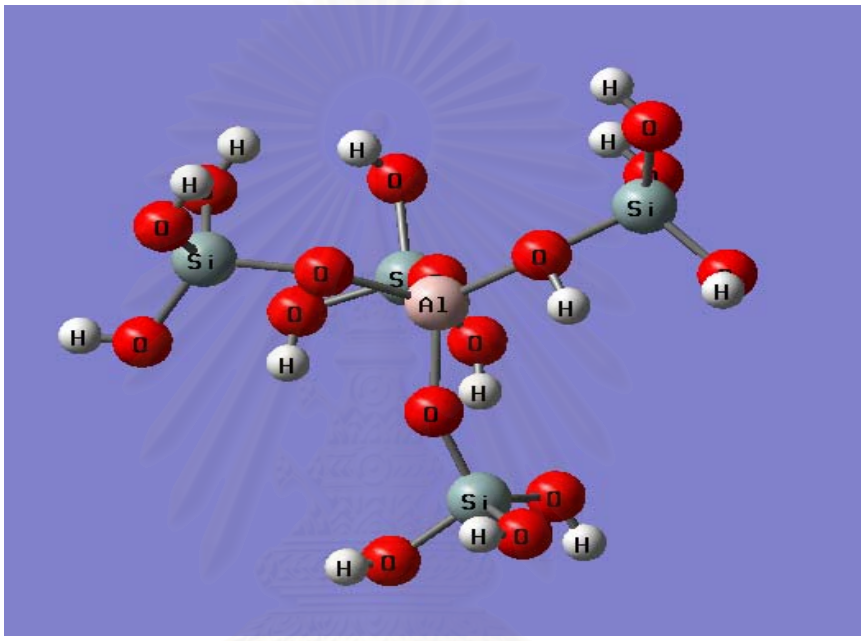

Figure 3.4 Cluster model for protonated ZSM-5 (ZH^+).

CHAPTER 4

RESULTS AND DISCUSSIONS

4.1 Structures of H-ZSM-5 with the Si/Al ratios of 47 and 95

4.1.1 Equilibrium Structures at 300 K

Structural properties obtained from MD simulation at 300 K for H-ZSM-5 with the Si/Al ratios of 47 and 95 and various Al substitutions were given. For H-ZSM-5 with the Si/Al ratio of 95, there were 12 sites studied and these geometrical parameters were listed in Table 4.1. For H-ZSM-5 with the Si/Al ratio of 47, there are 8 sites studied and these geometrical parameters were given in Table 4.2. These geometries are taken from the final structure of the simulations.

Table 4.1 Structural parameters of H-ZSM-5 with the Si/Al ratio of 95.

T1-site	Structural Parameters
Al-O (Å)	1.748
Si-O (Å)	1.602
O-Al-O (degree)	114.3
Al-O-Si (degree)	144.1
O-Si-O (degree)	101.5
Si-O-Si (degree)	157.2

Table 4.1 Structural parameters of H-ZSM-5 with the Si/Al ratio of 95. (Cont.)

T2-site	Structural Parameters
Al-O (Å)	1.773
Si-O (Å)	1.597
O-Al-O (degree)	115.0
Al-O-Si (degree)	139.3
O-Si-O (degree)	106.4
Si-O-Si (degree)	151.4

T3-site	Structural Parameters
Al-O (Å)	1.738
Si-O (Å)	1.645
O-Al-O (degree)	101.6
Al-O-Si (degree)	159.0
O-Si-O (degree)	104.7
Si-O-Si (degree)	156.9

T4-site	Structural Parameters
Al-O (Å)	1.716
Si-O (Å)	1.615
O-Al-O (degree)	111.3
Al-O-Si (degree)	154.1
O-Si-O (degree)	101.7
Si-O-Si (degree)	148.5

Table 4.1 Structural parameters of H-ZSM-5 with the Si/Al ratio of 95. (Cont.)

T5-site	Structural Parameters
Al-O (Å)	1.699
Si-O (Å)	1.626
O-Al-O (degree)	113.5
Al-O-Si (degree)	145.0
O-Si-O (degree)	106.0
Si-O-Si (degree)	136.5

T6-site	Structural Parameters
Al-O (Å)	1.729
Si-O (Å)	1.585
O-Al-O (degree)	108.0
Al-O-Si (degree)	133.5
O-Si-O (degree)	115.1
Si-O-Si (degree)	148.7

T7-site	Structural Parameters
Al-O (Å)	1.773
Si-O (Å)	1.591
O-Al-O (degree)	109.1
Al-O-Si (degree)	141.2
O-Si-O (degree)	109.9
Si-O-Si (degree)	154.1

Table 4.1 Structural parameters of H-ZSM-5 with the Si/Al ratio of 95. (Cont.)

T8-site	Structural Parameters
Al-O (Å)	1.676
Si-O (Å)	86.6
O-Al-O (degree)	109.4
Al-O-Si (degree)	161.5
O-Si-O (degree)	116.0
Si-O-Si (degree)	162.4

T9-site	Structural Parameters
Al-O (Å)	1.775
Si-O (Å)	1.568
O-Al-O (degree)	113.4
Al-O-Si (degree)	160.0
O-Si-O (degree)	112.7
Si-O-Si (degree)	155.8

T10-site	Structural Parameters
Al-O (Å)	1.706
Si-O (Å)	1.549
O-Al-O (degree)	111.2
Al-O-Si (degree)	131.7
O-Si-O (degree)	111.6
Si-O-Si (degree)	156.1

Table 4.1 Structural parameters of H-ZSM-5 with the Si/Al ratio of 95. (Cont.)

T11-site	Structural Parameters
Al-O (Å)	1.714
Si-O (Å)	1.568
O-Al-O (degree)	103.6
Al-O-Si (degree)	149.6
O-Si-O (degree)	104.8
Si-O-Si (degree)	145.7

T12-site	Structural Parameters
Al-O (Å)	1.790
Si-O (Å)	1.644
O-Al-O (degree)	106.2
Al-O-Si (degree)	145.0
O-Si-O (degree)	152.5
Si-O-Si (degree)	107.7

Table 4.2 Structural parameters of H-ZSM-5 with the Si/Al ratio of 47.

T4 in T4, T4* model	Structural Parameters
Al-O (Å)	1.763
Si-O (Å)	1.607
O-Al-O (degree)	108.6
Al-O-Si (degree)	143.6
O-Si-O (degree)	112.7
Si-O-Si (degree)	138.3

Table 4.2 Structural parameters of H-ZSM-5 with the Si/Al ratio of 47. (Cont.)

T4* in T4, T4* model	Structural Parameters
Al-O (Å)	1.766
Si-O (Å)	1.595
O-Al-O (degree)	104.5
Al-O-Si (degree)	111.9
O-Si-O (degree)	149.8
Si-O-Si (degree)	141.0

T5 in T5, T12 model	Structural Parameters
Al-O (Å)	1.697
Si-O (Å)	1.622
O-Al-O (degree)	99.5
Al-O-Si (degree)	141.9
O-Si-O (degree)	104.8
Si-O-Si (degree)	151.3

T12 in T5, T12 model	Structural Parameters
Al-O (Å)	1.744
Si-O (Å)	1.611
O-Al-O (degree)	115.0
Al-O-Si (degree)	150.9
O-Si-O (degree)	107.3
Si-O-Si (degree)	136.8

Table 4.2 Structural parameters of H-ZSM-5 with the Si/Al ratio of 47. (Cont.)

T6 in T6, T12 model	Structural Parameters
Al-O (Å)	1.746
Si-O (Å)	1.611
O-Al-O (degree)	113.8
Al-O-Si (degree)	142.9
O-Si-O (degree)	101.7
Si-O-Si (degree)	144.0

T12 in T6, T12 model	Structural Parameters
Al-O (Å)	1.770
Si-O (Å)	1.588
O-Al-O (degree)	109.8
Al-O-Si (degree)	146.1
O-Si-O (degree)	114.3
Si-O-Si (degree)	154.0

T7 in T7, T12 (model1)	Structural Parameters
Al-O (Å)	1.745
Si-O (Å)	1.610
O-Al-O (degree)	100.6
Al-O-Si (degree)	139.3
O-Si-O (degree)	104.1
Si-O-Si (degree)	158.7

Table 4.2 Structural parameters of H-ZSM-5 with the Si/Al ratio of 47. (Cont.)

T12 in T7, T12 (model1)	Structural Parameters
Al-O (Å)	1.736
Si-O (Å)	1.646
O-Al-O (degree)	120.7
Al-O-Si (degree)	140.1
O-Si-O (degree)	117.5
Si-O-Si (degree)	159.8

T7 in T7, T12 (model2)	Structural Parameters
Al-O (Å)	1.745
Si-O (Å)	1.614
O-Al-O (degree)	104.6
Al-O-Si (degree)	145.3
O-Si-O (degree)	107.0
Si-O-Si (degree)	147.1

T12 in T7, T12 (model2)	Structural Parameters
Al-O (Å)	1.736
Si-O (Å)	1.656
O-Al-O (degree)	18.6
Al-O-Si (degree)	141.4
O-Si-O (degree)	118.9
Si-O-Si (degree)	141.2

Table 4.2 Structural parameters of H-ZSM-5 with the Si/Al ratio of 47. (Cont.)

T7 in T7, T12 (model3)	Structural Parameters
Al-O (Å)	1.801
Si-O (Å)	1.707
O-Al-O (degree)	123.1
Al-O-Si (degree)	146.6
O-Si-O (degree)	106.9
Si-O-Si (degree)	160.7

T12 in T7, T12 (model3)	Structural Parameters
Al-O (Å)	1.749
Si-O (Å)	1.564
O-Al-O (degree)	109.8
Al-O-Si (degree)	154.4
O-Si-O (degree)	108.2
Si-O-Si (degree)	162.7

T8 in T8, T8* model	Structural Parameters
Al-O (Å)	1.812
Si-O (Å)	1.648
O-Al-O (degree)	110.4
Al-O-Si (degree)	144.8
O-Si-O (degree)	112.1
Si-O-Si (degree)	151.2

Table 4.2 Structural parameters of H-ZSM-5 with the Si/Al ratio of 47. (Cont.)

T8 in T8, T8* model	Structural Parameters
Al-O (Å)	1.795
Si-O (Å)	1.637
O-Al-O (degree)	108.2
Al-O-Si (degree)	144.2
O-Si-O (degree)	114.6
Si-O-Si (degree)	150.1

T9 in T9, T10 model	Structural Parameters
Al-O (Å)	1.783
Si-O (Å)	1.605
O-Al-O (degree)	116.3
Al-O-Si (degree)	143.5
O-Si-O (degree)	113.4
Si-O-Si (degree)	153.5

T10 in T9, T10 model	Structural Parameters
Al-O (Å)	1.773
Si-O (Å)	1.598
O-Al-O (degree)	108.5
Al-O-Si (degree)	152.6
O-Si-O (degree)	118.3
Si-O-Si (degree)	148.9

According to Tables 4.1 and 4.2, ZSM-5 with the Si/Al ratio of 95 have Al-O and Si-O distances in the ranges 1.676-1.790 and 1.549-1.645 Å, respectively. The O-Al-O, Al-O-Si, O-Si-O and Si-O-Si angles are 101.6-115.0, 131.7-161.5, 101.5-116.0, and 136.5-162.4 degree, respectively.

For ZSM-5 with the Si/Al ratio of 47, Al-O and Si-O are in the ranges of 1.697-1.812 and 1.545-1.707 Å, respectively. The O-Al-O, Al-O-Si, O-Si-O and Si-O-Si are 99.5-123.1, 139.3-154.4, 101.7-118.9, and 136.8-162.7 degree, respectively.

Thus, different Al substitution and Si/Al ratio result in different geometries and energies (see in APPENDICES I and II) for ZSM-5 from MD simulation, the site effect is evident. The smaller Al atom causes some distortion in zeolites. The Al-O distance (1.676-1.812 Å) is longer than Si-O (1.545-1.707 Å) while O-Al-O angle (99.5-123.1 degree) is smaller than O-Si-O angle (101.5-118.9 degree).

4.1.2 Positions of H^+ (Brønsted proton) in H-ZSM-5

Positions of H^+ in ZSM-5 with different Si/Al ratio and Al substitutions are of interest. Here, this feature is measured by O...H^+ distance, a distance between H^+ and O adjacent to Al substitutions, which is obtained from MD simulations. However, there are large numbers of configurations in the MD simulations and final structures might not be the best structure representing ZSM-5, especially for position of mobile H^+. The most probable O...H^+ distance is measured from the RDF of the simulations (see in APPENDIX III). The most probable O...H^+ distance or "RDF O...H^+ distance" is the more accurate measure for position of H^+. Table 4.3 displays O...H^+ distance of H-ZSM-5 with the Si/Al ratios of 47 and 95 and different Al substitutions. The notation *Max* refers to the longest distance, *Min* refers to the shortest distance and RDF refers to distance to the maximum of the O...H^+ RDF yielded from MD simulations.

From Table 4.3, the range of O...H^+ distance is indeed very narrow for all T-sites and the Si/Al ratio which suggested a very strong interaction between O and H^+.

Table 4.3 The *Max*, *Min* and RDF O...H^+ distance of H-ZSM-5.

Si/Al ratio	T-site	*Max* (Å)	*Min* (Å)	RDF (Å)
95	T1	1.067	0.928	0.997
	T2	1.038	0.934	0.989
	T3	1.075	0.927	0.993
	T4	1.049	0.919	0.985
	T5	1.052	0.914	0.982
	T6	1.065	0.924	0.985
	T7	1.054	0.931	0.993
	T8	1.071	0.925	0.994
	T9	1.059	0.928	0.983
	T10	1.054	0.931	0.991
	T11	1.059	0.918	0.986
	T12	1.054	0.938	0.998
47	T4,T4	1.072,1.064	0.937,0.938	0.999,0.999
	T5,T12	1.048,1.069	0.934,0.924	0.987,0.991
	T6,T12	1.038,1.027	0.920,0.928	0.994,0.988
	T7,T12 (model1)	1.065,1.103	0.925,0.904	0.986,0.988
	T7,T12 (model2)	1.055,1.055	0.936,0.936	0.994,0.994
	T7,T12 (model3)	1.078,1.071	0.937,0.907	1.000,0.987
	T8,T8	1.044,1.055	0.934,0.926	0.988,0.986
	T9,T10	1.073,1.055	0.913,0.937	0.991,1.000

4.2 Acidity of H-ZSM-5

Total energies in a.u. of protonated and unprotonated H-ZSM-5 cluster models with the Si/Al ratios of 95 and 47 were given in Tables 4.4 and 4.5 respectively.

Table 4.4 Energies in a.u. of protonated, E (ZH^+) and unprotonated, E (Z) ZSM-5 cluster models with the Si/Al ratio of 95 computed using B3LYP/6-31G (d, p).

T-sites	E (ZH^+)	E (Z)
1	-2612.52326	-2611.87892
2	-2612.54692	-2611.91026
3	-2612.54963	-2611.90782
4	-2612.52113	-2611.91587
5	-2612.55265	-2611.90670
6	-2612.56730	-2611.90499
7	-2612.53015	-2611.88006
8	-2612.55447	-2611.91245
9	-2612.57116	-2611.93153
10	-2612.54202	-2611.90810
11	-2612.53504	-2611.90245
12	-2612.55219	-2611.91368

Table 4.5 Energies in a.u. of protonated, E (ZH^+) and unprotonated, E (Z) ZSM-5 cluster models with the Si/Al ratio of 47 computed using B3LYP-6-31G (d, p).

T-sites	E (ZH^+)	E (Z)
T4*,T4	-2612.53589	-2611.90256
T4,T4*	-2612.54782	-2611.90458
T5*,T12	-2612.52016	-2611.88265
T5,T12*	-2612.54396	-2611.90115
T6*,T12	-2612.53454	-2611.90426
T6,T12*	-2612.53187	-2611.89853
T7*,T12 (model1)	-2612.55965	-2611.90757
T7,T12* (model1)	-2612.51450	-2611.88639
T7*,T12 (model2)	-2612.54329	-2611.90156
T7,T12* (model2)	-2612.54423	-2611.91325
T7*,T12 (model3)	-2612.54019	-2611.90442
T7,T12* (model3)	-2612.54363	-2611.90896
T8*,T8	-2612.58758	-2611.93610
T8,T8*	-2612.55402	-2611.91562
T9*,T10	-2612.57189	-2611.92617
T9,T10*	-2612.50638	-2612.88986

Table4.6 The proton affinity of ZSM-5 with the Si/Al ratios of 95 and 47 computed using energy from Tables 4.4 and 4.5.

Si/Al ratio	T-site	Proton affinity (ΔPA) (kcal/mol)
95	T1	405.8
	T2	398.0
	T3	401.1
	T4	400.6
	T5	388.8
	T6	414.8
	T7	405.5
	T8	401.0
	T9	398.2
	T10	401.3
	T11	394.2
	T12	402.4
47	T4,T4	394.6, 398.1
	T5,T12	397.1, 400.7
	T6,T12	392.4,398.5
	T7,T12 (model1)	408.3,395.1
	T7,T12 (model2)	402.7, 393.3
	T7,T12 (model3)	403.0,392.5
	T8,T8	412.7,402.5
	T9,T10	391.8,401.1

For H-ZSM-5 with the Si/Al ratio of 95 (see Table 4.6), values of PA were found to be between 388.8 and 414.8 kcal/mol. T5-substitution has the smallest PA while T6-site has largest PA. The smaller PA means more acidic because the proton can easily escape. Thus, Al substitution at T5-site gives the most acidic ZSM-5 whileT6-site is the least acidic. The T12 substitution has PA value is 402.4 kcal/mol, the intermediate between the smallest and largest PA. Since T12-site is at intersection between straight and sinusoidal channel, this T-site would play crucial role in catalytic activity of H-ZSM-5. [10]

In the case of H-ZSM-5 with the Si/Al ratio of 47, the value of PA was found that between 391.8 and 412.7 kcal/mol. For disubstituted ZSM-5, PAs at 2 Al substitutions are not equal. Thus, H^+ at different Al substitutions has different acidity. The smallest PA is for T9-site in T9, T10 substitution and the largest PA is for T8 in T8, T8*.

When compared PA at the same T-site in mono- and di-substituted ZSM-5, we found no trends. The PA at some T-sites becomes larger while the PA at some other T-sites becomes smaller for the disubstitution. However, there is one tendency observed *i.e.* PA of all T-site substitutions for ZSM-5 with the Si/Al ratio of 95 are smaller than those of 47 ratio. Thus, ZSM-5 with the Si/Al ratio of 95 is more acidic than that with the Si/Ai ratio of 47. In addition, we also found that at T12-site for all substitutions of the disubstituted ZSM-5 are always lower than that of the monosubstituted one. Thus, double Al substitutions make H^+ at T-12site more acidic.

The acid strength of ZSM-5 can be estimated by comparing PA of ZSM-5 with the known acid. Here, we chose acetic acid in aqueous solution in which pKa is 4.74. The computed PA for CH_3COOH (aq) is 415.00 kcal/mol. Thus, all ZSM-5 have lower acidity than acetic acid in aqueous solution.

CHAPTER 5

CONCLUSIONS AND SUGGESTIONS

5.1 Conclusions

1) Equilibrium Structures of H-ZSM-5 with Si/Al ratio of 47 and 95 at 300K

The equilibrium structures obtained from MD simulation at 300K, were found that for H-ZSM with the Si/Al ratio of 95, the geometrical parameters Al-O were in the range of 1.676 to 1.790 Å and Al8-O has the shortest distance and Al12-O has the longest distance. And the geometrical parameters Si-O were in the range of 1.549 to 1.645 Å where the parameter Si-O in T0-site has the shortest distance and Si-O in T3-site has the longest. For H-ZSM with the Si/Al ratio of 47, the geometrical parameters Al-O were between 1.697 and 1.812 Å where the parameter Al5-O in T5, T12 model has the shortest distance and Al8-O in T8, T8* model has the longest. While the geometrical parameters Si-O were between 1.545 and 1.707 Å where the parameter Si-O of T6-site in T6, T12 model has the shortest distance and Si-O of T7 in T7, T12 model3 has the longest.

H-ZSM-5 with the Si/Al ratio of 95 have parameters O-Al-O, Al-O-Si, O-Si-O and Si-O-Si angle are between 101.6-115.0, 131.7-161.5, 101.5-116.0, and 136.5-162.4 degrees, respectively. ZSM-5 with the Si/Al ratio of 47 have parameters O-Al-O, Al-O-Si, O-Si-O and Si-O-Si angle are in the ranges of 99.5-123.1, 139.3-154.4, 101.7-118.9, and 136.8-162.7 degrees, respectively.

2) Positions of H^+ (Brønsted proton) in H-ZSM-5

For H-ZSM-5 with the Si/Al ratio of 95, the O...H^+ distances were in the range of 0.914 to 1.075 Å, T5-site has the minimum distance and T3-site has the maximum distance. T12 substitution has largest RDF of O…H^+ distance 0.998 Å while T5 substitution has smallest RDF

O…H^+ distance 0.982 Å. For H-ZSM-5 with the Si/Al ratio of 47, the O...H^+ distances were in the range of 0.904 to 1.078 Å, T12 in T7, T12 (model1) has the minimum distance and T12 in T7, T12 (model3) has the maximum distance. T7-site in T7, T12 (model3) and T10-site in T9, T10 has highest RDF O...H^+ distance (1.000 Å while T7-site in T7, T12 (model1) and T8*-site in T8, T8* substitution has shortest (0.986 Å).

3) Acidity of H-ZSM-5

For H-ZSM-5 with the Si/Al ratio of 95, the values of PA were found to be between 388.8 and 414.8 kcal/mol. T5-substituted ZSM-5 has the smallest PA gives the most acidic while T6-site has largest PA provides least acidic. The T12 substituted ZSM-5 has PA value is 402.4 kcal/mol, the intermediate between the smallest and largest PA. While H-ZSM-5 with the Si/Al ratio of 47, the value of PA was found that between 391.8 and 412.7 kcal/mol. The smallest PA is for T9-site in T9, T10 model and the largest PA is for T8 in T8, T8* model. Thus, T9-site in T9, T10 model is the most acidic and T8 in T8, T8* model is the least acidic.

When compared PA at the same T-site between ZSM-5 with the Si/Al ratios of 95 and 47, we found no trends. However, there is one tendency observed *i.e.* PA at T12-substitution for all substitutions of the disubstituted ZSM-5 are always lower than that of the monosubstituted one. Thus, double Al substitutions make H^+ at T-12site more acidic. For T12-site, ZSM-5 with the Si/Al ratio of 47 is more acidic than ZSM-5 with the Si/Al ratio of 95.

5.2 Suggestions

Further work, study of acidity of H-ZSM-5 with other metal substitution such as B, Cu, Fe, Ga, and Ti etc. which called metallosilicate should be investigated..

REFERENCES

1. Demuth, T.; Hafner, J.; Benco, J.; and Toulhoat, H. “Structural and Acidic Properties of Modernite: An ab initio Density-Fuctional Study”, J. Phys. Chem. B, 104,(2000): 4593.
2. Volmer, J.M.; Truong T.N. “Mechanics of Hydrogen Exchange of Methane with H-Zeolite Y: An ab Initio Embedded Cluster Study”.104, (2000): 6308.
3. Barthoment, D. “Acidic Catalysts with Zeolites.” Zeolites Science and Technology (Reberio F.R. et al.). Martinus Nijhoff Publishers, the Hauge. (1984): 317.
4. Ashton, A.G.; Batamanian, S.; and Dwyer, J. “Acidity in Zeolites.” Catalysis by Acid and Bases (Imelik, B. et al.). Elsevier, Amsterdam. (1985):101-109.
5. Ricchiardi, G.; and Newsam, J.M. “Predicted Effects of Site-Specific Aluminum Substitution on the Framework Geometry and Unit Cell Dimensions of Zeolite ZSM-5 Materials.” J. Phys. Chem. B. Vol. 101, (1997): 9943.
6. Sano, T., Fujisawa, K.; and Higiwara, H. “High Stream Stability of HZSM-5 Type Zeolite Containing Alkaline Earth Metals.” Studies in Surface Science and Catalysis. Vol. 34, (1987). 613-624.
7. Olson, D.H.; Kokotailo, G.T.; and Lawton, S.L. “Crystal Structure-Related Properties of ZSM-5.” J. Phys. Chem. Vol. 85, (1981): 2238.
8. Windsor, C.M. “Computational Studies of Zeolite Catalysis.” Continuation Report: Zeolite Catalysis. (10^{th} Ed), (1998).
9. Teraishi, K.; Ishida, M.; Irisawa, J.; and Miyamoto, A. “Active Site Structure of Cu-ZSM-5: Computational Study.” Journal of Physical Chemistry B. Vol. 101, (1997): 8079-8080.
10. Gonzales, N.O.; Bell T.O.; and Chakraborty, A.K. “Density Functional Theory Calculations of the Effects of Local Composition and Defect Structure on the Proton Affinity of H-ZSM-5.” J. Phys. Chem. B. 101, (1997): 10058-10064.
11. Flanigen, E.M. “Zeolites and Molecular sieves: a Historical Perspective”. Stud. Sur. Sci. Catal. Netherlands: Elsevier Science Publishing, 58, (1991): 13-34.

12. Breck, D.W. “Zeolite Molecular Sieves”. New York: Robert E. Krieger Publishing., (1984): 635, 749.
13. Tanabe, K.; Misona, M.; Ona, Y.; and Hattori, H. “New solid Acids and Bases”. (Delman, B., and Yates, J.T.,eds.). Studies in Surface Science and Catalysis. Tokyo : Elsevier, 51, (1989): 142-161.
14. Corma, A.; Lemos, F.; Naccache, C.; and Ribeiro, F.R.”Zeolite Microporous Solid: Synthesis, Structure, and Reactivity”. E.G. Kluwer Academic Publishers. Dortrecht, the Netherlands, (1991): 373.
15. Kokotailo, G.T. “Zeolite Crystallography”. In F.R. Riberiro et al. (eds.) Zeolites: Science and Technology, Netherlands: Martinus Nijhoff Publishers, (1984): 83-108.
16. Szostak, R. Molecular Sieves: Principles of Synthesis and Identification. New York : Van Nostrand Reinhold, (1989).
17. Derouane, E.G. New Aspect of Molecular Shape Selectivity. Catalysis by Zeolites, (Lmelik, B. et al), Elsvier, Amsterdam, (1980).
18. Meier, W.M.; and Olsen, D.H.; Atlas of zeolite Structure Type. International Zeolite Association, IZA, Zurich, (1978).
19. Ashton, A.G.; Batmanian, S.; and Dwyer, J. “Acidities in Zeolites.” Catalysis by Acid and Bases (Imelik, B. et al.), Elsvier, Amsterdam, (1985): 101-109.
20. Barthoment, D., “Acidic catalysis Zeolites.” Zeolites Science and Technology (Rebeiro F.R. et al.), Martinus Nijhoff Publishers, the Huge, (1984): 317-346.
21. Tanabe, K.; Misona, M.; Ona, Y.; and Hattori, H. “New Solid Acids and Bases.” (Deiman, B., and Yates, J.T., eds.), Studies in Surface and Catalysis, Elsevier, Tokyo, 51, (1989): 142-161.
22. Dyer, A. “Zeolite Active Sites.” Introduction to Zeolite Molecular Sieves. Wiley, Cluchester, (1988): 121-124.
23. Gates, B.C. “Zeolite Molecular Sieves.” Catalytic Chemistry Singapore: John Wiley & Sons, (1992).
24. Mark, A. R; Geoge, C. S. “Quantum Mechanics.” Introduction to Quantum Mechanics in Chemistry. Prentice: New Jersey, (2000).

25. Szabo, A.; Ostlund, N. S. “The Born-Oppenheimer Approximation.” Modern Quantum Chemistry: Introduction to Advanced Electronic Structure Theory. MacMillan Publishing Co., New York, (1982).

26. Christopher J.C. “Ab initio Implementations of Hatree-Fock Molecular Orbital Theory.” Essentials of Computational Chemistry: Theories and Models, John-Wiley & Sons, Ltd., (2002): 153-188.

27. Jonathan, M.G. “Molecular Orbital Theory” Chemical Applications of Molecular Modeling, Royal Society of Chemistry, (1998).

28. Hehre, W.J.; Random, L.; Schleyer, P.R.; and Pople, J.A. “Ab initio Method.” Ab initio Molecular Orbital Theory, (1986).

29. David, C.Y. “Density Functional Theory” Computational Chemistry: A Practical Guide for Applying Techniques to Real World problems, A John Wiley & Sons, Inc., Publication, (2001).

30. Andrew, R.L. “Molecular Dynamics Simulation Methods.” Molecular Modeling: Principle and Applications. Prentice Hall, 2nd Ed, (2001): 353-406.

31. Frank, J. “Simulation Method” Introduction to Computational Chemistry. John-Wiley & Sons, (1999).

32. Sukrat, K. “Exchange of Copper Species in the Cavity of H-ZSM-5 at High Copper Loading” Master’s Thesis, Chemistry, Faculty of Science, Chulalongkorn University, Thailand, (2004).

APPENDICES

APPENDIX I

Minimization

```
    Minimize: Successful completion
    Maximum derivative              = 0.000931
    Last method used                = Conjugate Gradient (Polak_Ribiere)
    Total number of iterations      = 354
    Total number of function calls  = 704
    CPU time used                   = 14.08 seconds

MINIMIZATION ENERGY SUMMARY
_____________________________
                                 Initial                  Final
                                 -------                  -----
   Total Potential energy      -9475.985063          -11681.783312
   Internal                      958.123445            1088.534817
   bond                          233.860754             217.465477
   angle                         377.997652             566.466936
   torsion                       316.185804             273.204032
   out_of_plane                    0.000000               0.000000
   cross                          30.079235              31.398372
   bond_bond                      62.357192              25.130268
   bond_angle                    -32.277956               6.268104
   end_bond_torsion                0.000000               0.000000
   middle_bond_torsion             0.000000               0.000000
   angle_torsion                   0.000000               0.000000
   angle_angle_torsion             0.000000               0.000000
   bond_bond_1_3                   0.000000               0.000000
   angle_angle                     0.000000               0.000000
   torsion_torsion                 0.000000               0.000000
   oop_oop                         0.000000               0.000000
   nonbond                    -10434.108508          -12770.318129
   vdW                           -346.905083            -317.509207
   vdW_repulsive                  131.101566             117.749975
   vdW_dispersive                -478.006649            -435.259183
   electrostatic              -10087.203426          -12452.808922
   hydrogenbond                    0.000000               0.000000

Line  70:BTCL> writeFile coordinate filename = .cor

Total time used by DISCOVER: 14.89 secs

Completion date: Wed Sep  1 09:58:03 2004
Exiting Discover: status OK.
```

The output of minimization on H-ZSM-5 with the Si/Al ratio of 95 (T7-site)

Minimization (Cont.)

```
    Minimize: Successful completion
    Maximum derivative              = 0.000814
    Last method used                = Conjugate Gradient (Polak_Ribiere)
    Total number of iterations      = 330
    Total number of function calls  = 660
    CPU time used                   = 13.78 seconds

MINIMIZATION ENERGY SUMMARY
```

	Initial	Final
Total Potential energy	-9041.128789	-11405.052262
Internal	1188.628518	1191.971705
bond	347.026777	160.971273
angle	476.467092	737.180074
torsion	320.241939	275.725307
out_of_plane	0.000000	0.000000
cross	44.892711	18.095051
bond_bond	77.843984	13.206047
bond_angle	-32.951273	4.889004
end_bond_torsion	0.000000	0.000000
middle_bond_torsion	0.000000	0.000000
angle_torsion	0.000000	0.000000
angle_angle_torsion	0.000000	0.000000
bond_bond_1_3	0.000000	0.000000
angle_angle	0.000000	0.000000
torsion_torsion	0.000000	0.000000
oop_oop	0.000000	0.000000
nonbond	-10229.757307	-12597.023967
vdW	-346.905082	-330.184362
vdW_repulsive	131.101566	133.073570
vdW_dispersive	-478.006649	-463.257931
electrostatic	-9882.852225	-12266.839605
hydrogenbond	0.000000	0.000000

```
Line  70:BTCL> writeFile coordinate filename = .cor

Total time used by DISCOVER: 14.58 secs

Completion date: Wed Sep  1 10:04:30 2004
Exiting Discover: status OK.
```

The output of minimization on H-ZSM-5 with the Si/Al ratio of 47 (T7, T12 (model1))

APPENDIX II

Energy

The 30 frames with the LOWEST property values are:

RANK	CONFIG NO	FRAME NO	CONFORMER	Total Energy
1	10029	10029	10029	-11336.477539
2	13482	13482	13482	-11332.780273
3	6592	6592	6592	-11332.151367
4	17834	17834	17834	-11332.129883
5	17724	17724	17724	-11332.124023
6	14528	14528	14528	-11332.032227
7	12662	12662	12662	-11331.595703
8	8934	8934	8934	-11331.465820
9	11379	11379	11379	-11331.396484
10	14133	14133	14133	-11331.197266
11	17988	17988	17988	-11331.109375
12	14428	14428	14428	-11331.023438
13	13938	13938	13938	-11330.696289
14	15064	15064	15064	-11330.569336
15	16595	16595	16595	-11330.567383
16	17628	17628	17628	-11330.566406
17	6284	6284	6284	-11330.521484
18	7062	7062	7062	-11330.520508
19	16867	16867	16867	-11330.471680
20	10335	10335	10335	-11330.338867
21	8658	8658	8658	-11330.229492
22	15191	15191	15191	-11330.028320
23	7498	7498	7498	-11330.013672
24	17971	17971	17971	-11330.009766
25	6132	6132	6132	-11329.926758
26	15956	15956	15956	-11329.875000
27	11093	11093	11093	-11329.864258
28	14398	14398	14398	-11329.511719
29	1665	1665	1665	-11329.403320
30	7533	7533	7533	-11329.396484

Statistics for Total Energy:

Average	= -11311.962891
Standard Deviation	= 6.143148
Moment of Skewness	= 0.174690
Moment of Kurtosis	= 0.274533
Minimum Value	= -11336.477539
Maximum Value	= -11282.316406

Total Energy	Frequency
-11335.124023	0.000056
-11332.416016	0.000056
-11329.708008	0.001389
-11327.000000	0.003444
-11324.291992	0.013833
-11321.583008	0.036167
-11318.875000	0.072833
-11316.166992	0.121111
-11313.458984	0.161667
-11310.750977	0.173056
-11308.042969	0.159000
-11305.334961	0.121944
-11302.626953	0.073000
-11299.918945	0.035167
-11297.210938	0.015667
-11294.502930	0.006500
-11291.794922	0.002944
-11289.086914	0.001056
-11286.378906	0.000833
-11283.670898	0.000278

The output of minimum energy and configuration of H-ZSM-5 with the Si/Al ratio of 47 at T7,T12 (model1) were obtained from MD.

Energy (Cont.)

The 30 frames with the LOWEST property values are:

RANK	CONFIG NO	FRAME NO	CONFORMER	Total Energy
1	13701	13701	13701	-11546,600586
2	11346	11346	11346	-11545,150391
3	6963	6963	6963	-11543,864258
4	6761	6761	6761	-11543,549805
5	1881	1881	1881	-11543,308594
6	625	625	625	-11543,299805
7	9727	9727	9727	-11543,018555
8	6135	6135	6135	-11542,960938
9	2238	2238	2238	-11542,935547
10	8340	8340	8340	-11542,931641
11	1257	1257	1257	-11542,709961
12	7545	7545	7545	-11541,970703
13	7415	7415	7415	-11541,939477
14	13857	13857	13857	-11541,817383
15	10570	10570	10570	-11541,482422
16	12714	12714	12714	-11541,450195
17	7146	7146	7146	-11541,437500
18	2965	2965	2965	-11541,291992
19	14895	14895	14895	-11541,263672
20	15314	15314	15314	-11541,244141
21	1651	1651	1651	-11541,225586
22	16758	16758	16758	-11541,214844
23	6965	6965	6965	-11541,058594
24	5288	5288	5288	-11540,992188
25	5388	5388	5388	-11540,968750
26	8304	8304	8304	-11540,909180
27	7499	7499	7499	-11540,858398
28	2434	2434	2434	-11540,832031
29	2414	2414	2414	-11540,774414
30	1205	1205	1205	-11540,771484

Statistics for Total Energy:

Average = -11526,495117
Standard Deviation = 4,943819
Moment of Skewness = -0,012685
Moment of Kurtosis = -0,008781
Minimum Value = -11546,600586
Maximum Value = -11505,920898

Total Energy	Frequency
-11545,583984	0,000050
-11543,549805	0,000150
-11541,515625	0,000500
-11539,481445	0,003700
-11537,448242	0,009400
-11535,414062	0,023050
-11533,379883	0,047050
-11531,345703	0,079600
-11529,311523	0,121650
-11527,277344	0,148250
-11525,244141	0,163550
-11523,209961	0,149300
-11521,175781	0,112450
-11519,141602	0,074650
-11517,107422	0,039100
-11515,073242	0,017600
-11513,040039	0,006550
-11511,005859	0,002450
-11508,971680	0,000700
-11506,937500	0,000250

The output of minimum energy and configuration of H-ZSM-5 with the Si/Al ratio of 95 at T5-site were obtained from MD.

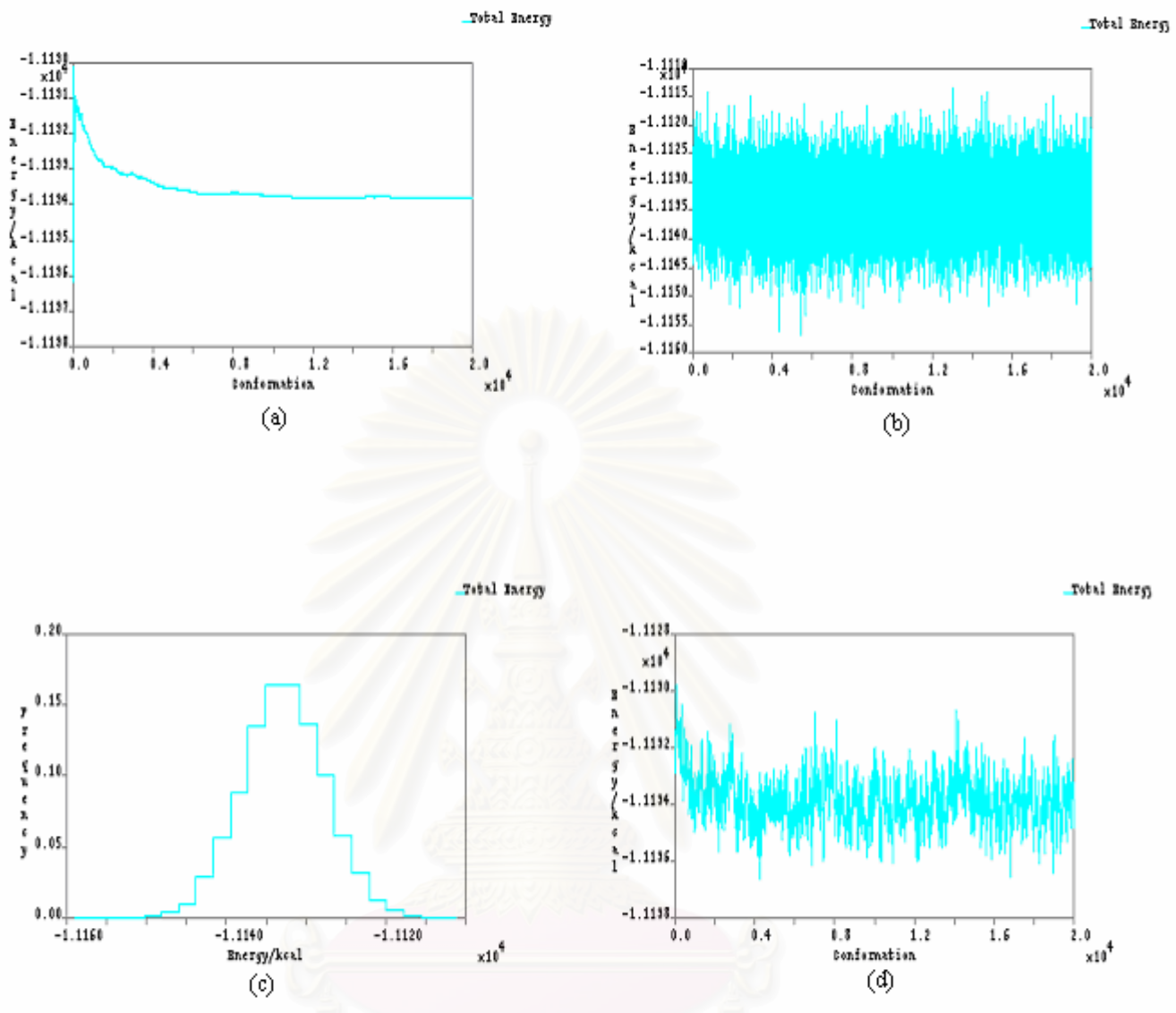

The graph of MD simulation on H-ZSM-5 with the Si/Al ratio of 47 (T6, T12)

(a) Running average

(b) Profile

(c) Distribution curve

(d) Block average

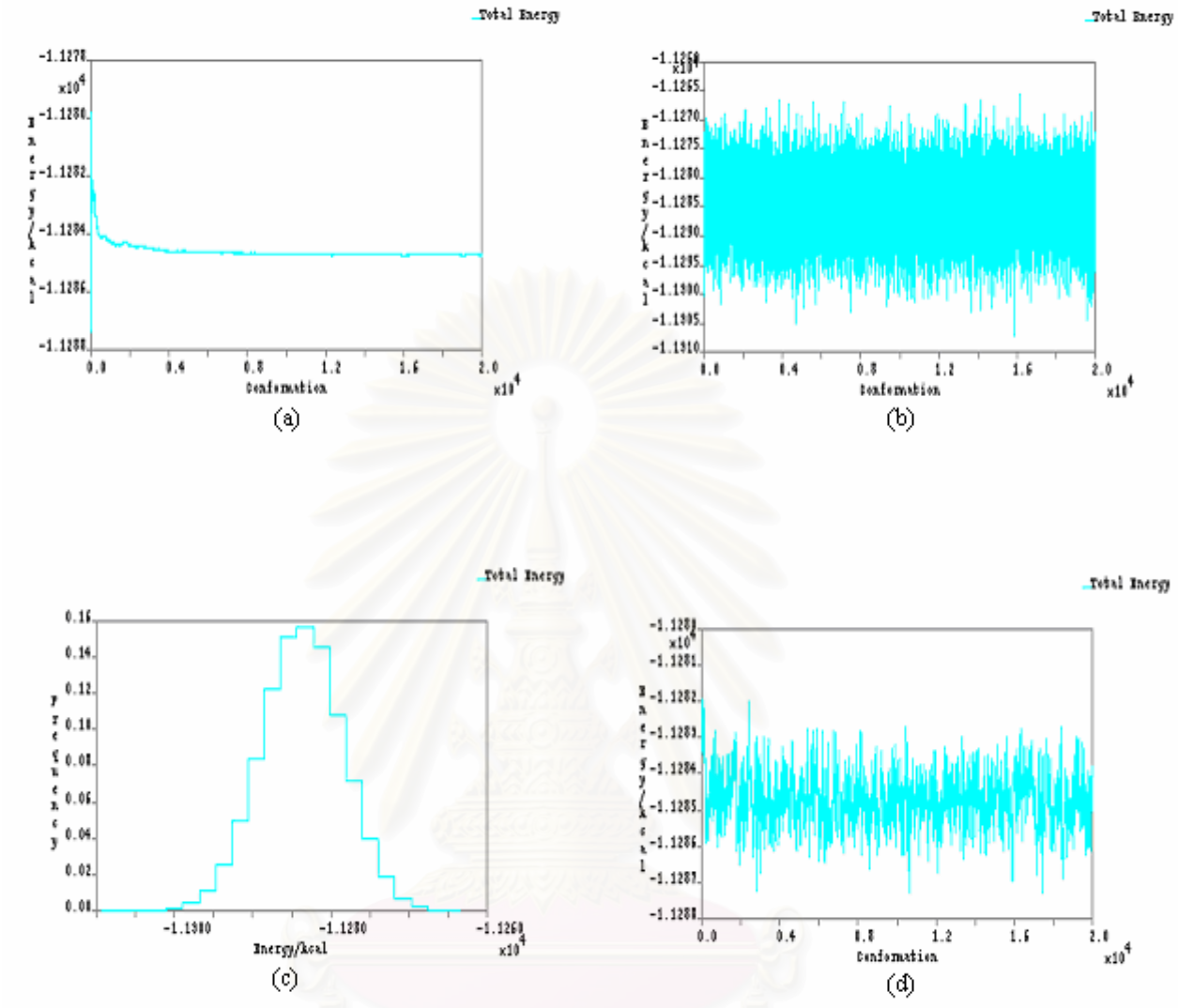

The graph of MD simulation on H-ZSM-5 with the Si/Al ratio of 47 (T9, T10)

(a) Running average

(b) Profile

(c) Distribution curve

(d) Block average

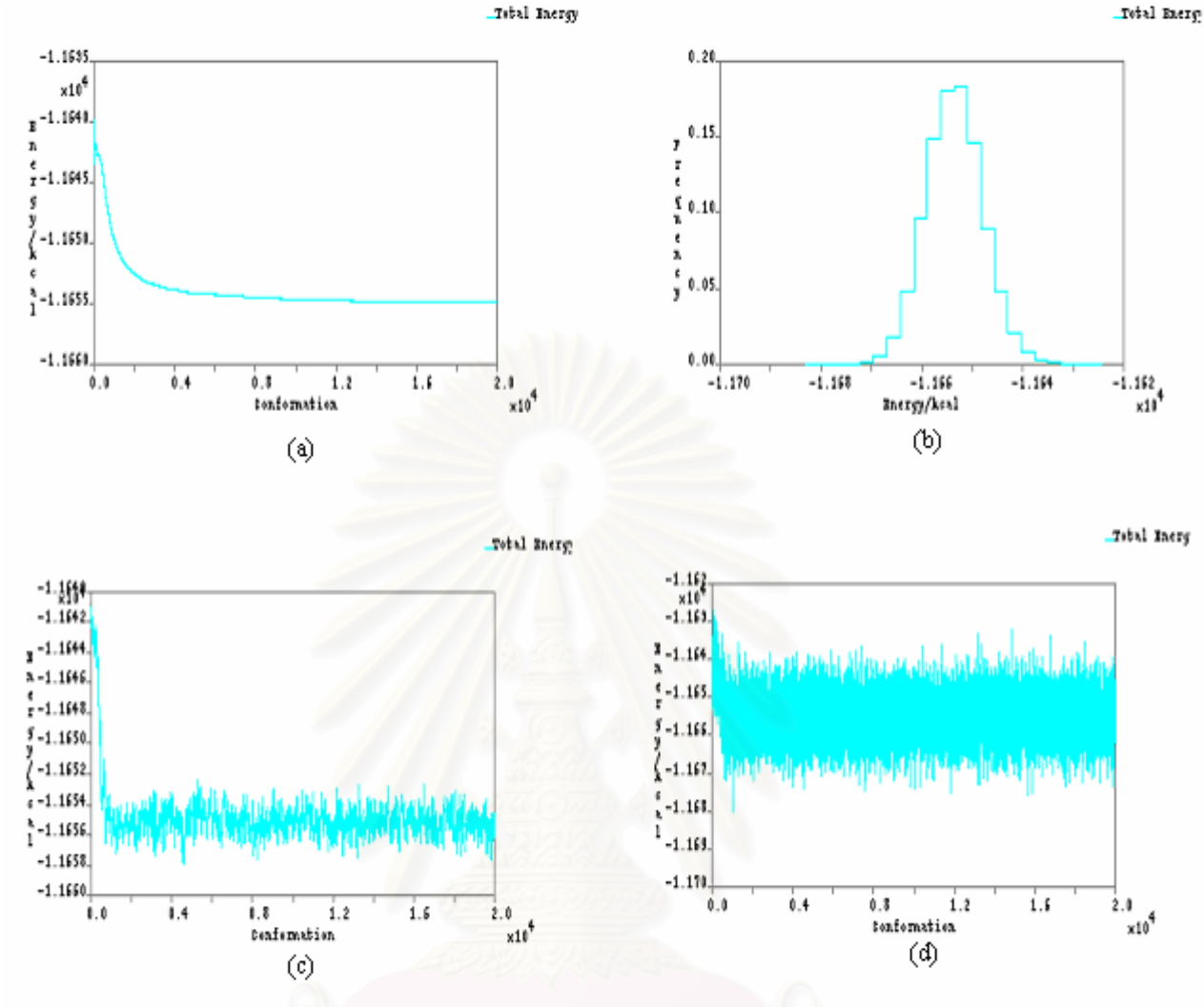

The graph of MD simulation on H-ZSM-5 with the Si/Al ratio of 95 (T1-site)

(a) Running average

(b) Distribution curve

(c) Block average

(d) Profile

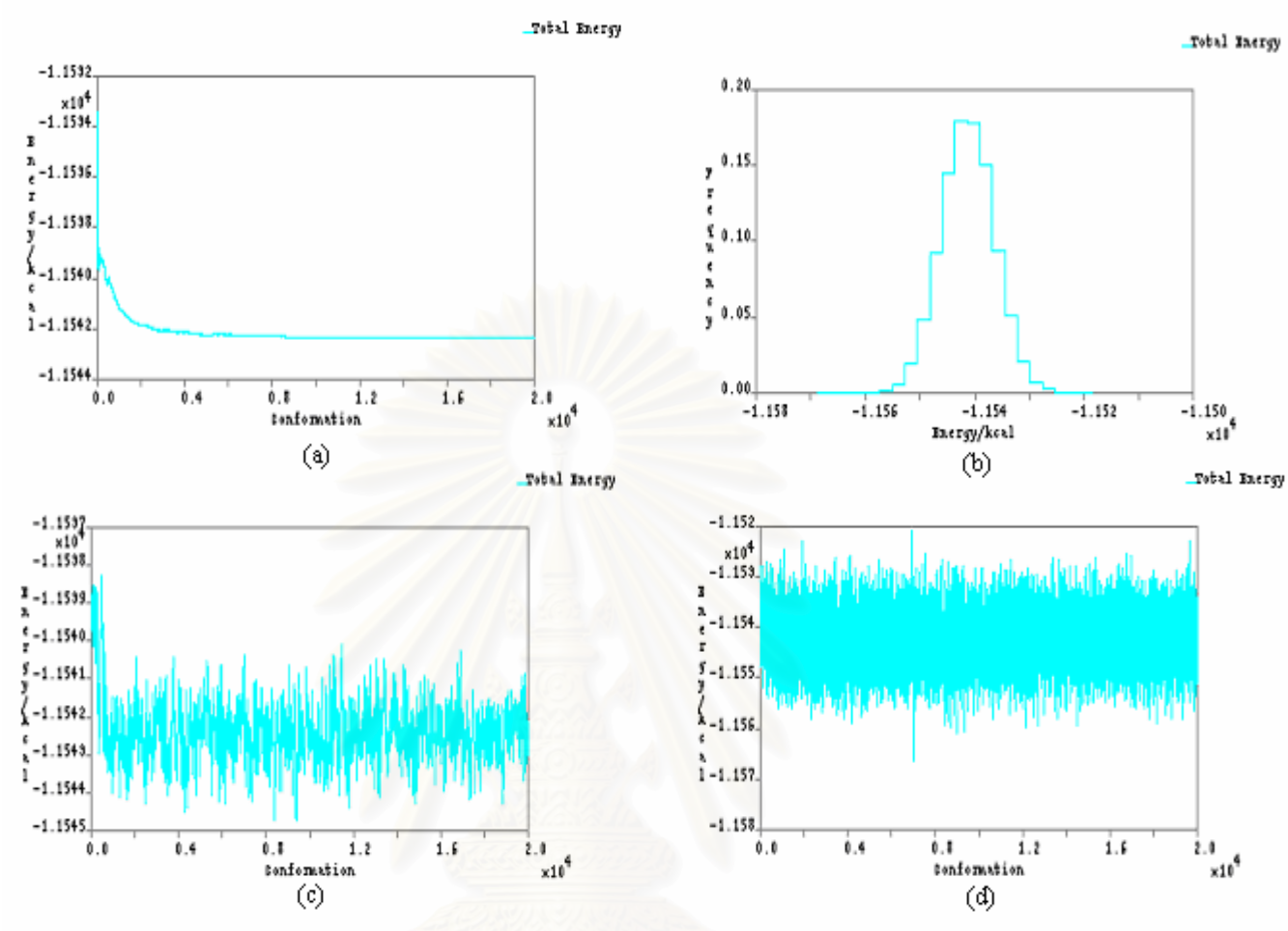

The graph of MD simulation on H-ZSM-5 with the Si/Al ratio of 95 (T4-site)

(a) Running average

(b) Distribution curve

(c) Block average

(d) Profile

APPENDIX III

Radial Distribution Function

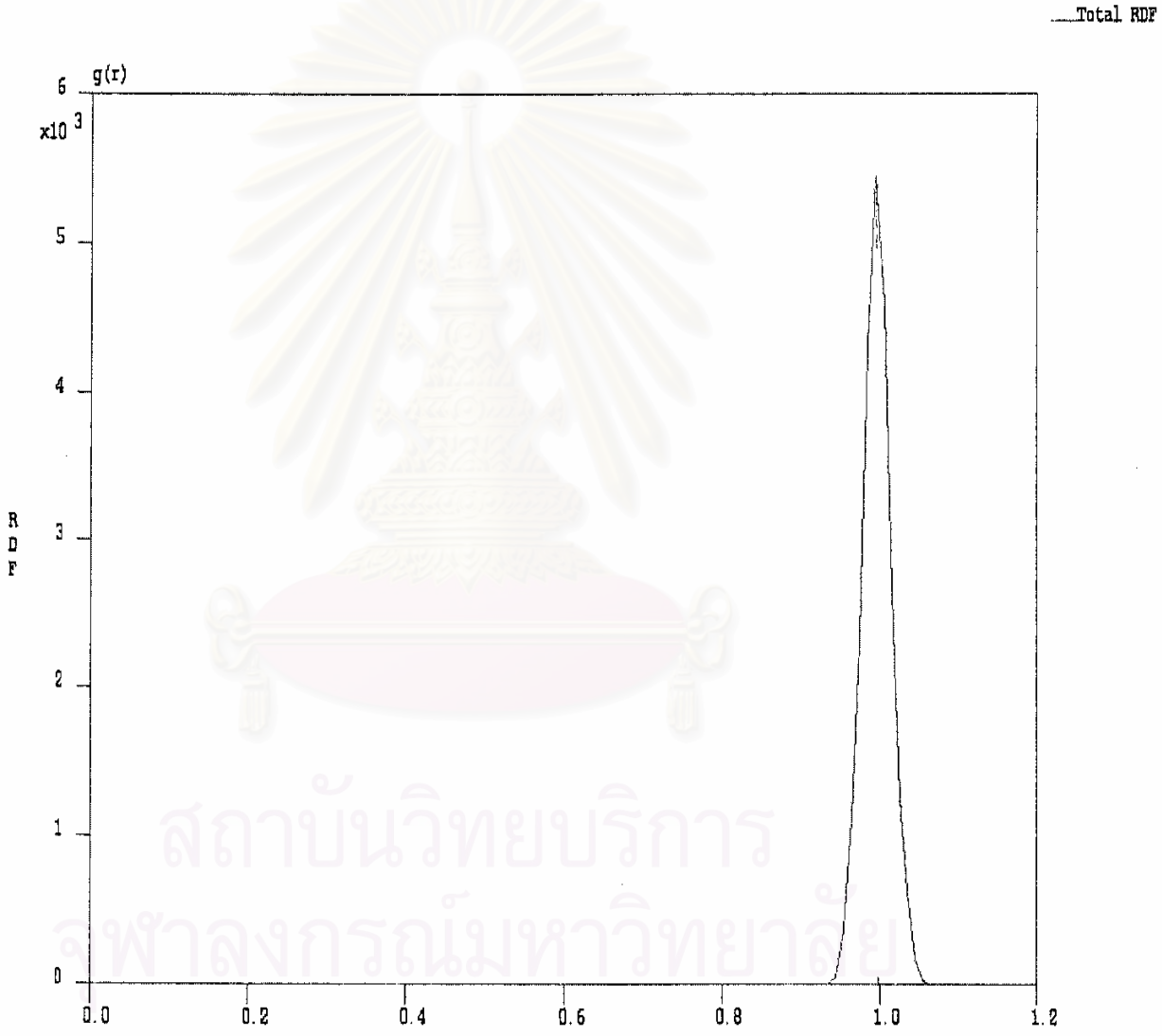

The RDF of O…H^+ bond distance of monosubstituted H-ZSM-5 (T11-site)

APPENDIX IV

MANUSCRIPT

STRUCTURES AND ACIDITIES OF HZSM-5 WITH Si/Al RATIOS OF 47 AND 95

Ukrid Poompub[1] and Vudhichai Parasuk[2]

ABSTRACT: ZSM-5 catalyst is widely used in petrochemical industry. Its catalytic activity depends on its acidity. ZSM-5 can be prepared at several silicon to aluminum ratio (Si/Al) and their acidities depend on is ratio. In this work, an investigation on the acidity of ZSM-5 at 2 Si/Al ratios, *i.e.* 95 (monosubstituted) and 47 (disubstituted) were carried out. Using Molecular Dynamic Simulation (MD), structures of ZSM-5 at different Si/Al ratio and substitution patterns were prepared. It was found that the most stable structures of ZSM-5 with the Si/Al ratio of 95 have radial distribution function (RDF) O…H^+ distances (a property relates to acidity) from 0.982 to 0.998 Å, while those with the Si/Al ratio of 47 have these distances in the range of 0.986 to 1.000 Å. The energy differences between various ZSM-5 structures were determined to estimate relative stabilities of different Al substitutions. For the Si/Al ratio of 95, T12 substituted ZSM-5 has the longest O…H^+ distance while the substitution at T11 makes ZSM-5 the most stable. For the Si/Al ratio of 47, substitution at T7-site in T7, T12 (model3) and T10-site in T9, T10has the longest O…H^+ distance and at T7, T12 (model1) has ZSM-5 the most stable. Density functional theory has been used to determine the effects of local composition and structure on the proton affinity (PA) of HZSM-5. For ZSM-5 with the Si/Al ratio of 95 has PA between 388.8 and 414.8 kcal/mol. The T5 substitution has lowest PA which makes its highest acidity. While ZSM-5 with Si/Al ratio at 95, the value of PA between 391.8 and 412.7 kcal/mol. TheT9-site in T9, T10 model has lowest PA which makes its highest acidity.

KEYWORDS: ZSM-5, molecular dynamic simulations, acidity, proton affinity

1. INTRODUCTION

Zeolites are microporous aluminosilicates that are industrially important for their catalytic and molecular sieving properties.[1, 2]Their network of cavities and channels allows them to accommodate even moderately large molecules, and the presence of Al-substituted tetrahedral sites, with an associated H^+ being bound to a nearby O atom maintain charge neutrality, results in acidic properties useful in catalysis. Classical Brønsted and Lewis acid model of acidity have been used to classify the active sites on zeolites.[3, 4] Brønsted acidity is proton donor acidity; a trigonally co-ordinated alumina atom is an electron deficient and can accept an electron pair, therefore behaves as a Lewis acid. The nature of the distribution of aluminum over the framework cation sites (T-sites) in aluminosilicate zeolites is known to influence their catalytic performance.[5, 6] In general; the increase in Si/Al ratio will increase acidic strength and thermal stability of zeolite. Since the number of acidic OH groups depends on the number of aluminum in zeolite's framework, decrease in Al content is expected to reduce catalytic activity of zeolite.

ZSM-5, a synthetic zeolite currently accessible over a framework composition range 8 < Si:Al < ∞, with Si:Al = 25-100 being typical, is arguably the most technologically important zeolite. Examples of its use include the conversion of methanol to gasoline, dewaxing of distillates, and the interconversion of aromatic compounds. Also, ZSM-5 has been shown to process unusual

1 ***Program of Pertrochemistry, Faculty of Science, University of Chulalongkonr, Bangkok 10330, Thailand; E-mail address: ukrid_2001@hyahoo.com***

2 ***Department of Chemistry, Faculty of Science, University of Chulalongkorn.***

hydrophobicity, leading to potential applications in the separation of hydrocarbons from polar compounds, such as water and alcohol.[7] The general framework structural characteristics of ZSM-5(MFI-framework) and the closely related purely siliceous material silicalite are well-know. Silicate tetrahedra are interlinked to form 4-, 5- and 6-ring in characteristic pentasil cages and chains. The chain interconnections define a two-dimensional system of 10-ring channels, straight along [010] (see picture 1), but sinusoidal along [100].

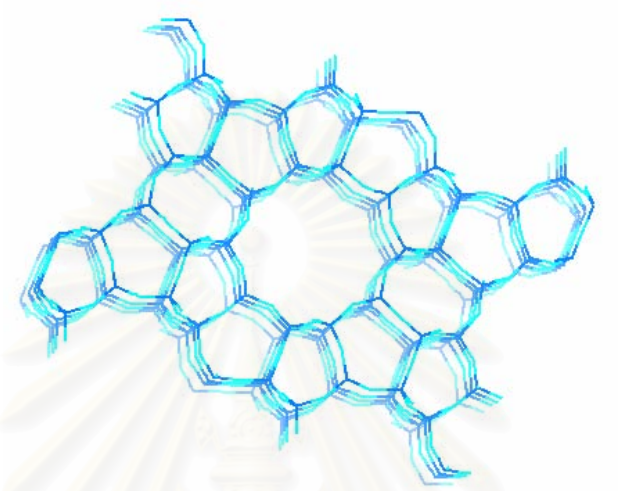

Figure1. Straight channel of ZSM-5 zeolite

It is clear that experimental techniques are lacking in some respect in the determination of zeolite structure and that other methods are needed to complete the picture.[8] Computational modeling is an ideal candidate to bridge this gap. Computational methods have proven to be invaluable in this area especially when used in collaboration with experimental work to verify the results. The majority of work published today in the zeolite field has some sort of theoretical calculation associated with it in one form or another. In cases where spectroscopic and crystallographic methods have failed to completely resolve a crystal structure, empirical force field method have been used to calculate minimum structures with aluminums explicitly placed. Molecular or lattice dynamics techniques have been used to measure sorption process through the zeolite pore channels. Electronic structure methods have also been used on small clusters to elucidate reaction pathways so that our understanding of zeolite chemistry can be increased with the aim of being able to predict how structural change will affect reactions.

In this work, acidities of ZSM-5 with the Si/Al ratios of 47 and 95 were studied. Molecular dynamic simulations of ZSM-5 with the Si/Al ratios of 47 and 95 were performed. The cluster models of difference T-site were made from structures obtained MD. The proton affinity (PA) of each model was completed to compare acidity between different T-sites.

2. METHODOLOGY

Initial X-ray structures of MFI-framework were taken from Crystal Builder in Cerius2 program package. By replacing Si atom with Al, model of ZSM-5 at 2 Si/Al ratio, *i.e.* 47 (disubstituted) and 95 (monosubstituted) were constructed. There are 12 T-sites for the Si/Al ratio of 95, *i.e.* T1, T2, T3, …, T12 and 8 T-sites for the Si/Al ratio of 47, *i.e.* T4,T4 , T5,T12 , T6,T12 , T7,T12(model1) , T7,T12(model2) , T7,T12(model3) (see picture 2), T8,T8 and T9,T10 being considered.[9] The substitution of Al onto each of these was accompanied by

placement of a proton at one of the four oxygen atoms of the $[AlO_4]^-$ tetrahedron, thus giving 12 and 8 different Al/H substitution configurations, respectively.

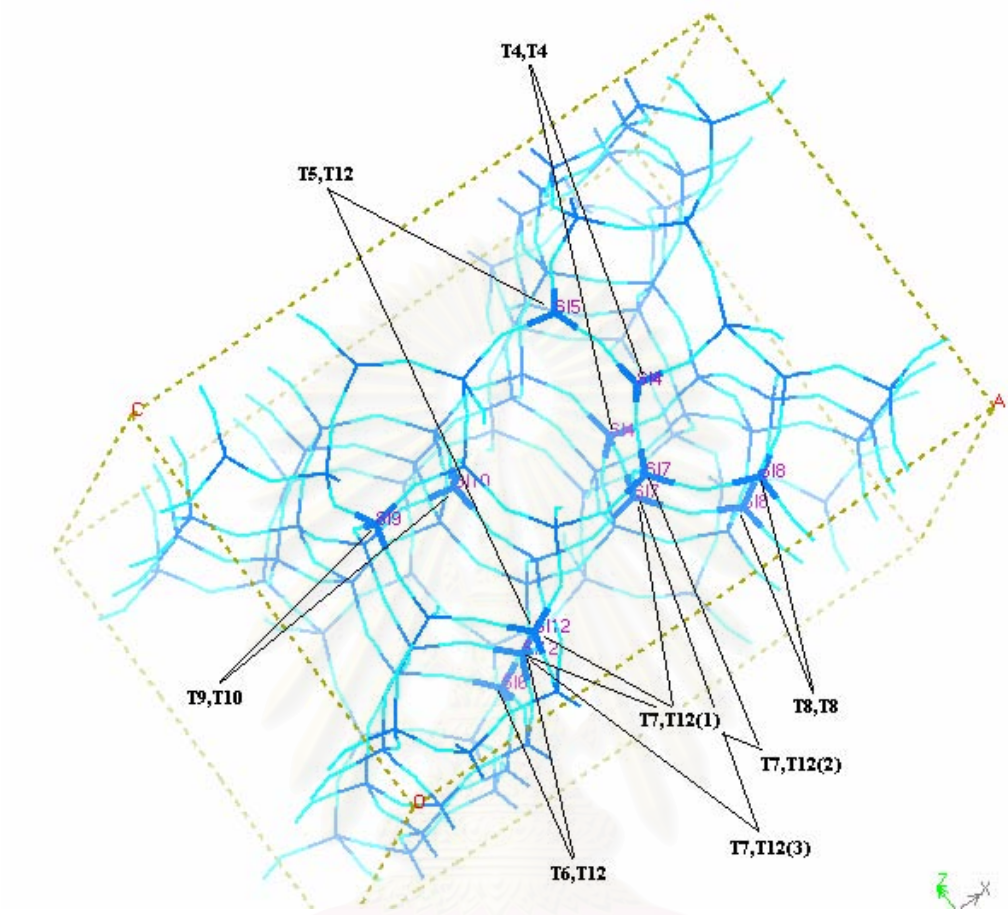

Figure2. The disubstitution on structures of ZSM-5 with Si/Al ratio at 47

Molecular dynamic (MD) simulations were performed with cvff force field using Discover module in Cerius2 program package. The NVE ensemble was performed for all structures at constant temperature 300 K. The equilibration time of 10 ps and run time of 2000 ps or until the system reaches equilibrium were used. Radial distribution function (RDF) of $O\ldots H^+$ distances for each structure was completed from trajectory file data. The B3LYP/6-31G (d,p) has been used to determine the effects of local composition and structure on the proton affinity (PA) of H-ZSM-5. These calculations were performed with clusters ranging in size from 33 to 34 atoms.

3. RESULTS AND DISCUSSION

The RDF of ZSM-5 with the Si/Al ratio of 95 is in the range of 0.982 to 0.998 Å. For ZSM-5 with the Si/Al ratio of 47, these distances are in the range of 0.986 to 1.000. It was found that among monosubstituted ZSM-5 T11 substitution has the lowest energy -11691.02 kcal/mol (force field energy from MD simulations). Thus, Al substitution at position T11 would form the most stable monosubstituted ZSM-5. Among disubstituted ZSM-5, T7, T12 (model1) substitution have the lowest energy -11336.48 kcal/mol. Therefore the substitution at T7, T12

(model1) positions would gave the most stable ZSM-5. For ZSM-5 with the Si/Al ratio of 95, value of PA were found to be between 388.8-414.8 kcal/mol, T5-site being the lowest and T6-site being highest. The lower of PA make the more acidic the ZSM-5. Thus, Al substitution at T5-site gives the most acidic zeolite. The T12 substitution yields PA of 402.4 kcal/mol. It is intermediate between the lowest and highest PA. The T12-site is at intersection and near around to play crucial role in catalytic activity.

Table1. The RDF distances of O…H^+ bond and proton affinity of protonated ZSM-5 with Si/Al ratio of 95 and 47

Si/Al ratio	T-site	RDF of O…H^+ distance (Å)	Proton affinity (ΔPA) (kcal/mol)
95	T1	0.997	405.8
	T2	0.989	398.0
	T3	0.993	401.1
	T4	0.985	400.6
	T5	0.982	388.8
	T6	0.985	414.8
	T7	0.993	405.5
	T8	0.994	401.0
	T9	0.983	398.2
	T10	0.991	401.3
	T11	0.986	394.2
	T12	0.998	402.4
47	T4,T4	0.999,0.999	394.6, 398.1
	T5,T12	0.987,0.991	397.1, 400.7
	T6,T12	0.994,0.988	392.4,398.5
	T7,T12 (model1)	0.986,0.988	408.3,395.1
	T7,T12 (model2)	0.994,0.994	402.7, 393.3
	T7,T12 (model3)	1.000,0.987	403.0,392.5
	T8,T8	0.988,0.986	412.7,402.5
	T9,T10	0.991,1.000	391.8,401.1

For ZSM-5 with the Si/Al ratio of 47, value of PA were found to be between 391.8 and 412.7 kcal/mol, in similar range to single substitution. The T-site with lowest PA is T9-site in T9, T10 substitution. However, the T6, T12 substitution has PA of 392.4(for T6-site) and 398.5(for T12-site). The disubstitution increase the acidity of ZSM-5 as compared to corresponding monosubstitution. The disubstitution not only provides stronger acidity by number of proton and also by proton itself. The O…H^+ distances often concludes with acid strength (and thus PA). However, no correlation was found between O…H^+ distances and PA. Thus, acidity of ZSM-5 is more complicate than being determined by only O…H^+ distance.

4. CONCLUSIONS

This work presents effects of Al substitution. For ZSM-5 with the Si/Al ratio of 95, T12 substitution have highest RDF, this site would provide high catalytic activity. The lowest energy is T11 which make it most stable structure. Where those ZSM-5 with the Si/Al ratio of 47, T7-site in T7, T12 (model3) and T10-site in T9,T10 is highest RDF distance and acidity while T7,T12 (model1) substitution has most stable structure. The proton affinity of H-ZSM-5 is found to depend on the local composition and structure of the zeolite in the vicinity of the Brønsted acid site. For ZSM-5 with the Si/Al ratio at 95, T5 substitution has lowest PA which makes its highest acidity and T6-site has lowest acidity. While ZSM-5 with the Si/Al ratio at 47, T9-site in T9, T10 model has highest acidity and T8-site in T8,T8 model lowest acidity.

REFERENCES

1. Catlow, C.R.A. (1992). Modeling of Structure and Reactivity in Zeolite. Academic, London.
2. Dyer, A. (1988). Introduction to Zeolite Molecular Sieves. Wiley, Cluchester.
3. Barthoment, D. (1984). “Acidic Catalysts with Zeolites.” Zeolites Science and Technology. Martinus Nijhoff Publishers, The Hauge.
4. Ashton, A.G., Batamanian, S., and Dwyer, J. (1985). “Acidity in Zeolites.” Catalysis by Acid and Bases. Elsevier, Amsterdam.
5. Ricchiardi, G., and Newsam, J.M. (1997). “Predicted Effects of Site-Specific Aluminum Substitution on the Framework Geometry and Unit Cell Dimensions of Zeolite ZSM-5 Materials.” Journal of Physical Chemistry B. Vol. 101, 9943.
6. Sano, T., Fujisawa, K., and Higiwara, H. (1987). “High Stream Stability of HZSM-5 Type Zeolite Containing Alkaline Earth Metals.” Studies in Surface Science and Catalysis. Vol. 34.
7. Olson, D.H., Kokotailo, G.T., and Lawton, S.L. (1981). “Crystal Structure-Related Properties of ZSM-5.” Journal of Physical Chemistry. Vol. 85, 2238.
8. Barthomeuf, D., Derouane, E.G., and Holderich, W. (1990). Guidelines for Mastering the Properties of Molecular Sieves. Plenum, New York, Vol. 221.
9. Windsor, C.M. (1998) “Computational Studies of Zeolite Catalysis.” Continuation Report: Zeolite Catalysis. (10^{th} Ed). March.
10. Teraishi, K., Ishida, M., Irisawa, J., and Miyamoto, A. (1997) “Active Site Structure of Cu-ZSM-5: Computational Study.” Journal of Physical Chemistry B. Vol. 101, 8079-8080.

VITAE

Ukrid Poompub

Born January 20th, 1980 in Bangkok, Thailand

Education

1986 - 1991 Primary Schools (Krongtupbokupathum Suesansongkrawe School, Bangkok, Thailand)

1992 - 1994 Secondary School (Samsenwitthayalai School, Bangkok, Thailand)

1995 - 1996 High School (Samsenwitthayalai School, Bangkok, Thailand)

1997 - 2000 Bachelor of Science (Chemistry), King's Mongkut University of Technology Thonburi (KMUTT), Bangmod, Thailand

2001 - 2004 Master of Science (Petrochemistry and polymer science) Chulalongkorn University, Bangkok, Thailand